Journal of Computational Mathematics
Vol.xx, No.x, 2024, 1–29.

http://www.global-sci.org/jcm
doi:10.4208/jcm.2212-m2022-0122

PROXIMAL ADMM APPROACH FOR IMAGE RESTORATION WITH MIXED POISSON-GAUSSIAN NOISE*

Miao Chen
Department of Mathematics, Nanchang University, Nanchang 330031, China
Department of Public Teaching, Quzhou College of Technology, Quzhou 324000, China
Yuchao Tang[1)]
School of Mathematics and Information Science, Guangzhou University, Guangzhou 510006, China
Email: yctang@gzhu.edu.cn
Jie Zhang
Department of Mathematics, The University of Hong Kong, Hong Kong SAR, China
Tieyong Zeng
Department of Mathematics, The Chinese University of Hong Kong, Shatin,
Hong Kong SAR, China

Abstract

Image restoration based on total variation has been widely studied owing to its edge-preservation properties. In this study, we consider the total variation infimal convolution (TV-IC) image restoration model for eliminating mixed Poisson-Gaussian noise. Based on the alternating direction method of multipliers (ADMM), we propose a complete splitting proximal bilinear constraint ADMM algorithm to solve the TV-IC model. We prove the convergence of the proposed algorithm under mild conditions. In contrast with other algorithms used for solving the TV-IC model, the proposed algorithm does not involve any inner iterations, and each subproblem has a closed-form solution. Finally, numerical experimental results demonstrate the efficiency and effectiveness of the proposed algorithm.

Mathematics subject classification: 65K10, 68U10, 94A08.
Key words: Image restoration, Mixed Poisson-Gaussian noise, Alternating direction method of multipliers, Total variation.

1. Introduction

Image restoration is a major problem in image processing, and its primary goal is to restore an original clean image from an observed image degraded by noise. Variational models are an important research direction for image restoration, wherein the basic idea is to construct an energy function according to a specific image restoration problem and minimize the energy function to obtain the original clear image. Generally, variational models include two items: a data fidelity item, which is established based on the probability distribution of noise, and a regularization item, which reflects prior information of the original image. Owing to the common influence of photon counting and thermal noise on the detector, observed images are often corrupted by mixed Poisson-Gaussian noise. Over the past two decades, researchers have extensively investigated the elimination of mixed Poisson-Gaussian noise. Consequently, the results of these studies have been applied to several practical problems, such as fluorescence

* Received May 8, 2022 / Revised version received August 29, 2022 / Accepted December 8, 2022 / Published online March 10, 2024 /
1) Corresponding author

microscopy images, X-ray computed tomography, and hyperspectral images. For more examples, the interested readers are recommended to refer to [2, 6, 9, 12, 20–22, 39] and the references therein.

Compared with the problem of image restoration from single Gaussian noise or Poisson noise, the removal of mixed Poisson-Gaussian noise removal is more complex, owing to the need to establish a suitable data-fidelity term. Existing methods developed to address this issue can be divided into two categories. The first category involves a certain transformation in which the mixed Poisson-Gaussian noise is transformed into a single type of noise. Then, either a mainstream Gaussian denoising algorithm or Poisson denoising algorithm is used to denoise the image to obtain a clean image. Representative models include the generalized Anscombe transform model [18, 19, 25, 31], reweighted L^2 (WL^2) model [14, 29], and shifted Poisson model [10]. The advantage of such a type of model is that a large number of Gaussian denoising algorithms or Poisson denoising algorithms are available for selection. See, for example [1, 8, 30]. However, its biggest shortcoming is that the estimation of data fidelity in this type of model is not sufficiently accurate. The other category involves establishing a model directly based on the probability distribution of mixed Poisson-Gaussian noise. Based on the maximum a posteriori (MAP) estimation framework, Chouzenoux *et al.* [7] proposed an exact mixed Poisson-Gaussian model, in which a data fidelity term was established by combining the statistical characteristics of both Poisson and Gaussian noise. Additionally, they proved the convexity and gradient Lipschitz continuity of the data fidelity term. Simultaneously, the author employed this property to solve the model using the primal-dual splitting method. However, the exact mixed Poisson-Gaussian model needs to solve the infinite sum problem of the function term series; therefore, obtaining a numerically accurate solution is rather difficult. In contrast, the authors of [5, 17] proposed a total variation infimal convolution model by using the generalized joint MAP [17] estimation method. The TV-IC model has a simple formulation and low computational complexity. Additionally, it provides a good estimate of the mixed Poisson-Gaussian noise. Lanza *et al.* [17] proposed a primal-dual-based iterative algorithm to solve the TV-IC model. However, the algorithm requires Newton iterations to solve a nonlinear optimization subproblem, which significantly increases the amount of calculation required for the outer loop. Moreover, the convergence of the algorithm is not certain. Calatroni *et al.* [5] proposed a semi-smooth Newton algorithm to solve the TV-IC model. However, the algorithm is constrained by the use of Newton iterations to solve the subproblem, which renders it highly time-intensive. Zhang *et al.* [40] proposed a bilinear constraint-based ADMM (BCA) algorithm to solve the TV-IC model. However, the BCA algorithm requires inner iterations while solving subproblems. Besides, it is only suitable to denoise pure Poisson-Gaussian noise. Recently, Toader *et al.* [35] proposed a primal-dual hybrid gradient (PDHG) algorithm to solve the TV-IC model. However, this algorithm also involves a subproblem that must be solved using the Newton iteration method.

In addition to these two types of methods, data-driven deep learning models have also been applied to the mixed Poisson-Gaussian noise problem, and they have achieved good results. For example, Remez *et al.* [28] implemented a denoising model based on a class-aware strategy using a fully convolutional neural network. Although deep learning models exhibit superior performance compared to traditional variational models in some cases, they involve certain limitations in terms of network construction and model training. In particular, the generalization ability of deep learning models depends on the choice of the training dataset.

To overcome the complications encountered by existing algorithms in solving the TV-IC model, we propose a proximal bilinear constraint-based ADMM (PBCA) algorithm. The significant difference between the PBCA and BCA algorithms is the addition of proximal terms while solving the u subproblem. This approach can help avoid inner iterations caused by the BCA algorithm. Therefore, the proposed algorithm can be used to denoise and deblur with mixed Poisson-Gaussian noise. Further, we prove the convergence of the proposed algorithm under mild conditions. To demonstrate the efficiency and effectiveness of the proposed algorithm, we compare its performance with that of other image restoration algorithms on mixed Poisson-Gaussian noise.

The remainder of this paper is organized as follows. In Section 2, we briefly review the TV-IC model and the BCA algorithm. In Section 3, we introduce the proposed PBCA algorithm and prove its convergence. In Section 4, we present the results of numerical experiments conducted to demonstrate the efficiency and effectiveness of the proposed algorithm. Finally, we provide some concluding remarks in Section 5.

2. Review of the TV-IC Model and BCA Algorithm

In this section, first, we briefly review the TV-IC model proposed by [5,17]. We then discuss the BCA algorithm [40].

2.1. Review of the TV-IC model

Let $u \in R^{m\times n}$ be an ideal image, H be a blur operator, and w be additive Gaussian noise with zero mean and standard deviation σ. Suppose that the image $u \in R^{m\times n}$ is corrupted by mixed Poisson-Gaussian noise, that is, the observed image $f \in R^{m\times n}$ is obtained by

$$\begin{aligned} v &= \text{Poisson}(Hu), \\ f &= v + w. \end{aligned}$$

Based on the generalized joint MAP estimation method and Bayes' rule [16, 32], we have

$$\begin{aligned} (u^\star, v^\star) &= \operatorname*{argmax}_{u,v} \prod_i P(u_i, v_i | f_i) \\ &= \operatorname*{argmax}_{u,v} \prod_i \frac{P(f_i|u_i, v_i) P(u_i, v_i)}{P(f_i)} \\ &= \operatorname*{argmax}_{u,v} \prod_i P(f_i|u_i, v_i) P(v_i|u_i) P(u_i) \\ &= \operatorname*{argmax}_{u,v} \prod_i P(f_i|v_i) P(v_i|u_i) P(u_i). \end{aligned} \tag{2.1}$$

By combining the Poisson noise intensity function

$$P(v_i|u_i) = \frac{(Hu)_i^{v_i} e^{-(Hu)_i}}{v_i!},$$

the Gaussian noise intensity function

$$P(f_i|v_i) = e^{-\frac{|f_i - v_i|^2}{2\sigma^2}},$$

the prior density function $P(u_i) = e^{-\lambda\varphi(Lu_i)}$, and by further computing the negative logarithm of the general joint MAP estimate (2.1), we obtain

$$\begin{aligned}(u^\star, v^\star) &= \underset{u,v}{\operatorname{argmin}} - \ln\left(\prod_i P(f_i|v_i)P(v_i|u_i)P(u_i)\right)\\ &= \underset{u,v}{\operatorname{argmin}}\sum_i\big(- \ln P(f_i|v_i) - \ln P(v_i|u_i) - \ln P(u_i)\big)\\ &= \underset{u,v}{\operatorname{argmin}}\frac{1}{2\sigma^2}\sum_i(f_i - v_i)^2 + \sum_i\big((Hu)_i - v_i\ln(Hu)_i + \ln v_i!\big) + \lambda\sum_i\varphi(Lu_i). \end{aligned} \tag{2.2}$$

Thereafter, using the standard Stirling [26,27] approximation of the logarithm of the factorial function to v_i, we obtain the following TV-IC model, which was established in [5,17]:

$$\min_{u,v}\frac{\lambda_1}{2}\|f - v\|^2 + \lambda_2 KL(Hu, v) + \varphi(Lu) + \delta_U(u) + \delta_V(v), \tag{2.3}$$

where

$$\lambda_1 = \frac{1}{\lambda\sigma^2}, \quad \lambda_2 = \frac{1}{\lambda}, \quad KL(Hu, v) = \sum_i\left((Hu)_i - v_i - v_i\ln\frac{(Hu)_i}{v_i}\right),$$

and $\delta_U(u)$ is the indicator function of the constraint set $U = \{u|0 \le u_i \le \mathrm{M}, \forall i\}$ defined by

$$\delta_U(u) = \begin{cases} 0, & u \in U,\\ +\infty, & \text{otherwise.}\end{cases}$$

Additionally, $\delta_V(v)$ denotes the indicator function of the constraint set $V = \{v|v_i \ge \epsilon > 0, \forall i\}$. It should be noted that we require v to have a lower bound, which is introduced to evaluate the convergence guarantee of the proposed algorithm.

2.2. Review of the BCA algorithm

Zhang *et al.* [40] evaluated the TV-IC model (2.3) when $H = I$, that is,

$$\min_{u,v}\frac{\lambda_1}{2}\|f - v\|^2 + \lambda_2 KL(u, v) + \|\nabla u\|_1 + \delta_V(v), \tag{2.4}$$

where $\|\nabla u\|_1$ denotes the total variation. They proposed the BCA algorithm to solve (2.4), which is presented as

$$\begin{cases} u^{k+1} = \underset{u}{\operatorname{argmin}} L_\alpha(u, v^k, w^k, \Lambda^k),\\ v^{k+1} = \underset{v}{\operatorname{argmin}} L_\alpha(u^{k+1}, v, w^k, \Lambda^k),\\ w^{k+1} = \underset{w}{\operatorname{argmin}} L_\alpha(u^{k+1}, v^{k+1}, w, \Lambda^k),\\ \Lambda^{k+1} = \Lambda^k + \alpha(v^{k+1}\cdot w^{k+1} - u^{k+1}),\end{cases} \tag{2.5}$$

where $\cdot$ denotes element-wise multiplication, and L_α represents the augmented Lagrangian function defined by

$$\begin{aligned} L_\alpha(u, v, w, \Lambda) = {}& \frac{\lambda_1}{2}\|f - v\|^2 + \lambda_2\sum_i(u_i - v_i - v_i\ln w_i)\\ &+ \|\nabla u\|_1 + \delta_V(v) + \langle\Lambda, v\cdot w - u\rangle + \frac{\alpha}{2}\|v\cdot w - u\|^2.\end{aligned}$$

The convergence of the BCA algorithm (2.5) was established in [40]. To avoid the subproblem of minimizing the total variation of u in the BCA algorithm, Zhang *et al.* [40] further proposed a $\mathrm{BCA_f}$ algorithm (BCA with full splitting) as follows:

$$\begin{cases} u^{k+1} = \underset{u}{\operatorname{argmin}} L_{\alpha_w,\alpha_p}\big(u, v^k, w^k, p^k, \Lambda_w^k, \Lambda_p^k\big), \\ v^{k+1} = \underset{v}{\operatorname{argmin}} L_{\alpha_w,\alpha_p}\big(u^{k+1}, v, w^k, p^k, \Lambda_w^k, \Lambda_p^k\big), \\ w^{k+1} = \underset{w}{\operatorname{argmin}} L_{\alpha_w,\alpha_p}\big(u^{k+1}, v^{k+1}, w, p^k, \Lambda_w^k, \Lambda_p^k\big), \\ p^{k+1} = \underset{p}{\operatorname{argmin}} L_{\alpha_w,\alpha_p}\big(u^{k+1}, v^{k+1}, w^{k+1}, p, \Lambda_w^k, \Lambda_p^k\big), \\ \Lambda_w^{k+1} = \Lambda_w^k + \alpha_w(v^{k+1} \cdot w^{k+1} - u^{k+1}), \\ \Lambda_p^{k+1} = \Lambda_p^k + \alpha_p(p^{k+1} - \nabla u^{k+1}), \end{cases} \tag{2.6}$$

where $L_{\alpha_w,\alpha_p}(u, v, w, p, \Lambda_w, \Lambda_p)$ is defined as

$$\begin{aligned} L_{\alpha_w,\alpha_p}(u, v, w, p, \Lambda_w, \Lambda_p) = {}& \frac{\lambda_1}{2}\|f - v\|^2 + \lambda_2 \sum_i (u_i - v_i - v_i \ln w_i) \\ & + \|p\|_1 + \delta_V(v) + \langle \Lambda_w, v \cdot w - u\rangle + \frac{\alpha_w}{2}\|v \cdot w - u\|^2 \\ & + \langle \Lambda_p, p - \nabla u\rangle + \frac{\alpha_p}{2}\|p - \nabla u\|^2. \end{aligned}$$

However, the convergence of the $\mathrm{BCA_f}$ algorithm (2.6) remains uncertain.

3. Main Algorithm and Convergence Analysis

In this section, we propose a completely splitting algorithm to solve the TV-IC model (2.3). Following the idea of the BCA algorithm (2.5), by introducing an auxiliary variable $(Hu)_i = w_i \cdot v_i$, the resulting subproblem of u represents a total variation and least-square minimization problem, which does not have a closed-form solution. If the $\mathrm{BCA_f}$ algorithm (2.6) is used, a system of linear equations must be solved, and moreover, the theoretical convergence of the algorithm cannot be guaranteed. Therefore, by introducing the proximal term and using a smooth regularization function, we develop a completely splitting algorithm to solve the TV-IC model (2.3), with the advantage that each subproblem has a closed-form solution.

3.1. PBCA algorithm

First, by introducing two auxiliary variables, $(Hu)_i = w_i \cdot v_i$ and $Lu_i = y_i$ for any $1 \le i \le n$, we rewrite (2.3) as the following equivalent constrained problem:

$$\begin{aligned} & \min_{u,v,w,y} \frac{\lambda_1}{2}\|f - v\|^2 + \lambda_2 \sum_i (w_i \cdot v_i - v_i - v_i \ln w_i) + \varphi(y) + \delta_U(u) + \delta_V(v) \\ & \text{s.t.} \quad (Hu)_i = w_i \cdot v_i, \quad Lu_i = y_i, \quad \forall\, 1 \le i \le n. \end{aligned} \tag{3.1}$$

The augmented Lagrangian function of the constrained problem mentioned above is given as

$$\begin{aligned} L_{\rho_1,\rho_2}(u, v, w, y, d_1, d_2) = {}& \frac{\lambda_1}{2}\|f - v\|^2 + \lambda_2 \sum_i (w_i \cdot v_i - v_i - v_i \ln w_i) \\ & + \varphi(y) + \delta_U(u) + \delta_V(v) + \langle d_1, Hu - w \cdot v\rangle \\ & + \frac{\rho_1}{2}\|Hu - w \cdot v\|^2 + \langle d_2, Lu - y\rangle + \frac{\rho_2}{2}\|Lu - y\|^2, \end{aligned} \tag{3.2}$$

where $\rho_1 > 0$ and $\rho_2 > 0$ represent penalty parameters, d_1 and d_2 denote Lagrangian multipliers, $\langle \cdot, \cdot \rangle$, and $\|\cdot\|$ denote the inner product and norm, respectively, and $\cdot$ represents element-wise multiplication. In the remainder of this work, all multiplications, divisions, exponentiations, and square root operations considered are performed element-wise.

Then, based on the preconditioned ADMM [3, 4, 11, 13, 15, 23, 33, 36, 38] framework, we propose the following iterative algorithm to solve (3.1):

$$\begin{cases} u^{k+1} = \underset{u}{\operatorname{argmin}} L_{\rho_1,\rho_2}\big(u, v^k, w^k, y^k, d_1^k, d_2^k\big) + \frac{1}{2}\|u - u^k\|_P^2, \\ v^{k+1} = \underset{v}{\operatorname{argmin}} L_{\rho_1,\rho_2}\big(u^{k+1}, v, w^k, y^k, d_1^k, d_2^k\big), \\ w^{k+1} = \underset{w}{\operatorname{argmin}} L_{\rho_1,\rho_2}\big(u^{k+1}, v^{k+1}, w, y^k, d_1^k, d_2^k\big), \\ y^{k+1} = \underset{y}{\operatorname{argmin}} L_{\rho_1,\rho_2}\big(u^{k+1}, v^{k+1}, w^{k+1}, y, d_1^k, d_2^k\big), \\ d_1^{k+1} = d_1^k + \rho_1(Hu^{k+1} - w^{k+1} \cdot v^{k+1}), \\ d_2^{k+1} = d_2^k + \rho_2(Lu^{k+1} - y^{k+1}), \end{cases} \tag{3.3}$$

where P indicates a positive definite symmetric matrix. Now, we demonstrate that each subproblem in (3.3) has a closed-form solution.

First, we consider the u-subproblem as

$$\begin{aligned} u^{k+1} = \underset{u}{\operatorname{argmin}} \Big\{ & \delta_U(u) + \big\langle d_1^k, Hu - w^k \cdot v^k \big\rangle + \frac{\rho_1}{2}\|Hu - w^k \cdot v^k\|^2 \\ & + \big\langle d_2^k, Lu - y^k \big\rangle + \frac{\rho_2}{2}\|Lu - y^k\|^2 + \frac{1}{2}\|u - u^k\|_P^2 \Big\}. \end{aligned} \tag{3.4}$$

To obtain a closed-form solution to the u-subproblem, we define

$$P = \frac{1}{\alpha} I - \rho_1 H^\top H - \rho_2 L^\top L,$$

where $1 > \alpha(\rho_1\|H\|^2 + \rho_2\|L\|^2)$. Subsequently, the u-subproblem can be simplified into the following form:

$$\begin{aligned} u^{k+1} &= \underset{u}{\operatorname{argmin}} \Big\{ \delta_U(u) + \big\langle d_1^k, Hu \big\rangle + \frac{\rho_1}{2}\big(\langle Hu, Hu\rangle - 2\langle Hu, w^k \cdot v^k\rangle\big) + \big\langle d_2^k, Lu \big\rangle \\ &\qquad + \frac{\rho_2}{2}\big(\langle Lu, Lu\rangle - 2\langle Lu, y^k\rangle\big) + \frac{1}{2}\big(\langle u - u^k, Pu\rangle - \langle u - u^k, Pu^k\rangle\big) \Big\} \\ &= \underset{u}{\operatorname{argmin}} \Big\{ \delta_U(u) + \big\langle H^\top d_1^k, u \big\rangle + \frac{\rho_1}{2}\langle H^\top H u, u\rangle - \big\langle \rho_1 H^\top w^k \cdot v^k, u \big\rangle + \big\langle L^\top d_2^k, u \big\rangle \\ &\qquad + \frac{\rho_2}{2}\langle L^\top L u, u\rangle - \big\langle \rho_2 L^\top y^k, u \big\rangle + \frac{1}{2}\langle Pu, u\rangle - \big\langle Pu^k, u \big\rangle \Big\} \\ &= \underset{u}{\operatorname{argmin}} \Big\{ \delta_U(u) + \frac{1}{2\alpha}\big\|u - \alpha\big(Pu^k - H^\top d_1^k + \rho_1 H^\top w^k \cdot v^k - L^\top d_2^k + \rho_2 L^\top y^k\big)\big\|^2 \Big\}. \end{aligned}$$

Consequently, u^{k+1} can be easily computed by

$$u^{k+1} = P_U\big(\alpha\big(Pu^k - H^\top d_1^k + \rho_1 H^\top w^k \cdot v^k - L^\top d_2^k + \rho_2 L^\top y^k\big)\big), \tag{3.5}$$

where P_U represents an orthogonal projection onto the closed convex set U. For the definition $U = \{u|0 \leq u_{i,j} \leq \mathrm{M}\}$, we have

$$\big(P_U(u)\big)_{i,j} = \begin{cases} u_{i,j}, & \text{if} \quad 0 \leq u_{i,j} \leq \mathrm{M}, \\ 0, & \text{if} \quad u_{i,j} < 0, \\ \mathrm{M}, & \text{if} \quad u_{i,j} > \mathrm{M}. \end{cases}$$

Second, we consider the v-subproblem, which is given as

$$\begin{aligned} v^{k+1} = \underset{v}{\operatorname{argmin}} \Big\{ & \frac{\lambda_1}{2}\|f - v\|^2 + \lambda_2 \sum_i \big(w_i^k \cdot v_i - v_i - v_i \ln w_i^k\big) + \delta_V(v) \\ & + \big\langle d_1^k, Hu^{k+1} - w^k \cdot v \big\rangle + \frac{\rho_1}{2}\|Hu^{k+1} - w^k \cdot v\|^2 \Big\} \\ = \underset{v \geq \epsilon}{\operatorname{argmin}} \Big\{ & \frac{\lambda_1}{2}\|f - v\|^2 + \lambda_2 \sum_i \big(w_i^k \cdot v_i - v_i - v_i \ln w_i^k\big) \\ & + \big\langle d_1^k, Hu^{k+1} - w^k \cdot v \big\rangle + \frac{\rho_1}{2}\|Hu^{k+1} - w^k \cdot v\|^2 \Big\}. \end{aligned}$$

The abovementioned minimization problem can be calculated independently for each component of v, that is

$$\begin{aligned} v_i^{k+1} = \underset{v_i \geq \epsilon}{\operatorname{argmin}} \Big\{ & \frac{\lambda_1}{2}(f_i - v_i)^2 + \lambda_2 \big(w_i^k \cdot v_i - v_i - v_i \ln w_i^k\big) \\ & + \big\langle {d_1^k}_i, (Hu^{k+1})_i - w_i^k \cdot v_i \big\rangle + \frac{\rho_1}{2}\big((Hu^{k+1})_i - w_i^k \cdot v_i\big)^2 \Big\}. \end{aligned} \tag{3.6}$$

The optimality condition of (3.6) is

$$\big(\lambda_1 + \rho_1 \big(w_i^k\big)^2\big) \cdot v_i^{k+1} - \lambda_1 f_i + \lambda_2 \big(w_i^k - 1 - \ln w_i^k\big) - \rho_1 w_i^k \cdot (Hu^{k+1})_i - w_i^k \cdot {d_1}_i^k = 0.$$

Then, the optimal solution of the v-subproblem is

$$v^{k+1} = \max(\hat{v}^{k+1}, \epsilon),$$

where $\max(\cdot\,,\cdot)$ represents the maximum value of the two vectors and $\hat{v}^{k+1}$ is defined by

$$\hat{v}^{k+1} = \frac{\lambda_1 f + \lambda_2 (I + \ln w^k - w^k) + \rho_1 w^k \cdot Hu^{k+1} + w^k \cdot d_1^k}{\lambda_1 + \rho_1 (w^k)^2}.$$

Third, we consider the w-subproblem as

$$\begin{aligned} w^{k+1} &= \underset{w}{\operatorname{argmin}} \Big\{ \lambda_2 \sum_i \big(w_i \cdot v_i^{k+1} - v_i^{k+1} \cdot \ln w_i\big) + \big\langle d_1^k, Hu^{k+1} - w \cdot v^{k+1} \big\rangle \\ &\qquad + \frac{\rho_1}{2}\|Hu^{k+1} - w \cdot v^{k+1}\|^2 \Big\} \\ &= \underset{w}{\operatorname{argmin}} \Big\{ \lambda_2 \sum_i \big(w_i \cdot v_i^{k+1} - v_i^{k+1} \cdot \ln w_i\big) + \frac{\rho_1}{2}\Big\|Hu^{k+1} - w \cdot v^{k+1} + \frac{d_1^k}{\rho_1}\Big\|^2 \Big\}. \end{aligned}$$

The optimality condition for the abovementioned problem is

$$\rho_1\big(v_i^{k+1}\big)^2\cdot\big(w_i^{k+1}\big)^2+\big(\lambda_2 v_i^{k+1}-\rho_1 v_i^{k+1}\cdot(Hu^{k+1})_i-v_i^{k+1}\cdot {d_1}_i^k\big)\cdot w_i^{k+1}-\lambda_2 v_i^{k+1}=0. \tag{3.7}$$

Then, w^{k+1} can be easily computed as

$$w^{k+1}=\frac{-\big(\lambda_2-\rho_1 Hu^{k+1}-d_1^k\big)+\sqrt{\big(\lambda_2-\rho_1 Hu^{k+1}-d_1^k\big)^2+4\rho_1\lambda_2 v^{k+1}}}{2\rho_1 v^{k+1}}. \tag{3.8}$$

Finally, we consider the y-subproblem as

$$\begin{aligned}
y^{k+1}&=\underset{y}{\operatorname{argmin}}\left\{\varphi(y)+\langle d_2^k, Lu^{k+1}-y\rangle+\frac{\rho_2}{2}\|Lu^{k+1}-y\|^2\right\}\\
&=\underset{y}{\operatorname{argmin}}\left\{\varphi(y)+\frac{\rho_2}{2}\left\|y-\left(Lu^{k+1}+\frac{d_2^k}{\rho_2}\right)\right\|^2\right\}\\
&=\operatorname{prox}_{\frac{1}{\rho_2}\varphi}\left(Lu^{k+1}+\frac{d_2^k}{\rho_2}\right).
\end{aligned} \tag{3.9}$$

Therefore, each subproblem of the iterative algorithm (3.3) has a closed-form solution.

The following lemma indicates the relationship between w^{k+1} and d_1^{k+1}, and it can be used to simplify the calculation of the v-subproblem.

Lemma 3.1. *Let $\{w^{k+1}\}$ and $\{d_1^{k+1}\}$ be generated by* (3.3)*, then, we have*

$$w^{k+1}\cdot\big(\lambda_2-d_1^{k+1}\big)=\lambda_2.$$

Proof. According to the optimality condition of the w-subproblem (3.7) and the update rule of multiplier d_1, we obtain

$$\begin{aligned}
0&=\rho_1(v^{k+1})^2\cdot(w^{k+1})^2+\big(\lambda_2 v^{k+1}-\rho_1 v^{k+1}\cdot Hu^{k+1}-v^{k+1}\cdot d_1^k\big)\cdot w^{k+1}-\lambda_2 v^{k+1}\\
&=v^{k+1}\cdot w^{k+1}\big(\lambda_2-\rho_1(Hu^{k+1}-v^{k+1}\cdot w^{k+1})-d_1^k\big)-\lambda_2 v^{k+1}\\
&=v^{k+1}\cdot w^{k+1}\big(\lambda_2-d_1^{k+1}\big)-\lambda_2 v^{k+1}.
\end{aligned}$$

Because $v_i\geq\epsilon>0$ for any i, we obtain

$$w^{k+1}\cdot\big(\lambda_2-d_1^{k+1}\big)=\lambda_2.$$

The proof is complete. $\square$

By Lemma 3.1, we obtain

$$\begin{aligned}
\hat{v}^{k+1}&=\frac{\lambda_1 f+\lambda_2(I+\ln w^k-w^k)+\rho_1 w^k\cdot Hu^{k+1}+w^k\cdot d_1^k}{\lambda_1+\rho_1(w^k)^2}\\
&=\frac{\lambda_1 f+\lambda_2\ln w^k+\rho_1 w^k\cdot Hu^{k+1}+\lambda_2-w^k\cdot(\lambda_2-d_1^k)}{\lambda_1+\rho_1(w^k)^2}\\
&=\frac{\lambda_1 f+\lambda_2\ln w^k+\rho_1 w^k\cdot Hu^{k+1}}{\lambda_1+\rho_1(w^k)^2}.
\end{aligned}$$

Therefore, the calculation of v^{k+1} can be simplified as follows:

$$\begin{aligned}
v^{k+1}&=\max(\hat{v}^{k+1},\epsilon)\\
&=\max\left(\frac{\lambda_1 f+\lambda_2\ln w^k+\rho_1 w^k\cdot Hu^{k+1}}{\lambda_1+\rho_1(w^k)^2},\epsilon\right).
\end{aligned} \tag{3.10}$$

The following presents a summary of the proposed algorithm to solve the TV-IC model.

Algorithm 3.1: Proximal Bilinear Constraint-Based ADMM Algorithm to Solve the TV-IC Model.

Input : For arbitrary u^0, v^0, w^0, and y^0. Given $\lambda_1, \lambda_2, \rho_1$, and ρ_2.

1 Solve u^{k+1} by (3.5).
2 Solve v^{k+1} by (3.10).
3 Solve w^{k+1} by (3.8).
4 Solve y^{k+1} by (3.9).
5 Update the multipliers by

$$\begin{aligned} d_1^{k+1} &= d_1^k + \rho_1(Hu^{k+1} - w^{k+1} \cdot v^{k+1}), \\ d_2^{k+1} &= d_2^k + \rho_2(Lu^{k+1} - y^{k+1}). \end{aligned}$$

Stop when a given stopping criterion is satisfied.

Output: u^{k+1}.

3.2. Convergence analysis of the PBCA algorithm

In this subsection, we demonstrate the convergence of the proposed PBCA algorithm. To guarantee sufficient descent and boundedness of the iterative sequences generated by Algorithm 3.1, we assume the following.

Assumption 3.1. *H and L represent two bounded linear operators, and there exists a constant $\bar{c} > 0$ such that*

$$\|Hu\|^2 + \|Lu\|^2 \geq \bar{c}^2\|u\|^2$$

for any u.

Assumption 3.2. *The function φ is convex, coercive, smooth, and gradient Lipschitz continuous with constant L_φ, that is*

$$\|\nabla\varphi(x) - \nabla\varphi(y)\| \leq L_\varphi\|x - y\|.$$

Remark 3.1. Prior works established that the total variation $\|u\|_{TV}$ can be represented by a composition of a convex function φ (e.g. ℓ_1-norm) and a first-order difference operator L, i.e. $\|u\|_{TV} = \varphi(Lu)$. See, for example [24, 34]. However, the ℓ_1-norm is not differentiable. In this study, we choose Huber-TV (see (4.1)) as the regularization function, which satisfies Assumption 3.2.

We take advantage of the following lemma, and the proof of which can be found in [40].

Lemma 3.2. *Let*

$$T(x) = \frac{1}{2}\|Ax - b\|^2 + M(x),$$

where $M(x)$ denotes a convex function. Let $x^\star$ be a stationary point of $T(x)$, that is, $0 \in \partial T(x^\star)$, where $\partial T(x^\star)$ represents the subdifferential of $T(x)$ in the convex analysis sense. Then, we have

$$T(x) - T(x^\star) \geq \frac{1}{2}\|A(x - x^\star)\|^2.$$

We can now prove the convergence of Algorithm 3.1. The convergence can be divided into three steps.

Step 1. The size of the successive difference of the dual variable is controlled by the successive difference of the original variable.

Step 2. The augmented Lagrangian function $L_{\rho_1,\rho_2}(u^k, v^k, w^k, y^k, d_1^k, d_2^k)$ is a monotonically decreasing function with a lower bound.

Step 3. Combining with the previous two steps, we can prove that the algorithm converges to the stationary point solution.

Lemma 3.3. *Suppose that Assumption* 3.2 *holds. Let* $\{(w^{k+1}, y^{k+1}, d_1^{k+1}, d_2^{k+1})\}$ *be the sequences generated by Algorithm* 3.1*, and let the iterative sequence* $\{w^k\}$ *has a uniformly positive lower bound, that is,* $w_i^k \geq c > 0$ *for any* i*, where* c *denotes a positive constant that is independent of* k*. Then, we have*

$$\begin{aligned}
\left\|d_1^{k+1} - d_1^k\right\|^2 &\leq \frac{\lambda_2^2}{c^4}\|w^{k+1} - w^k\|^2, \\
\left\|d_2^{k+1} - d_2^k\right\|^2 &\leq L_\varphi^2\|y^{k+1} - y^k\|^2.
\end{aligned}$$

Proof. It follows from Lemma 3.1 that

$$\begin{aligned}
\left\|d_1^{k+1} - d_1^k\right\|^2 &= \left\|\frac{\lambda_2 w^{k+1} - \lambda_2}{w^{k+1}} - \frac{\lambda_2 w^k - \lambda_2}{w^k}\right\|^2 \\
&= \left\|\frac{(\lambda_2 w^{k+1} - \lambda_2)\cdot w^k - (\lambda_2 w^k - \lambda_2)\cdot w^{k+1}}{w^{k+1}\cdot w^k}\right\|^2 \\
&= \left\|\frac{\lambda_2(w^{k+1} - w^k)}{w^{k+1}\cdot w^k}\right\|^2 \\
&\leq \frac{\lambda_2^2}{c^4}\|w^{k+1} - w^k\|^2.
\end{aligned} \tag{3.11}$$

According to the first-order optimality condition of the y-subproblem, the following holds:

$$\nabla\varphi(y^{k+1}) - \left(d_2^k + \rho_2(Lu^{k+1} - y^{k+1})\right) = 0 \implies \nabla\varphi(y^{k+1}) = d_2^{k+1}.$$

Therefore, we deduce the following:

$$\left\|d_2^{k+1} - d_2^k\right\|^2 = \|\nabla\varphi(y^{k+1}) - \nabla\varphi(y^k)\|^2 \leq L_\varphi^2\|y^{k+1} - y^k\|^2.$$

The proof is complete. □

Lemma 3.4. *Suppose that Assumption* 3.2 *holds. Let* $\{(w^{k+1}, y^{k+1}, d_1^{k+1}, d_2^{k+1})\}$ *be the sequences generated by Algorithm* 3.1*, and let the iterative sequence* $\{w^k\}$ *has a uniformly positive lower bound. Let* $1 > \alpha(\rho_1\|H\|^2 + \rho_2\|L\|^2)$, $\rho_1 > \sqrt{2}\lambda_2/(\epsilon c^2)$ *and* $\rho_2 > \sqrt{2}L_\varphi$*. Then, we have*

$$\begin{aligned}
&L_{\rho_1,\rho_2}\left(u^k, v^k, w^k, y^k, d_1^k, d_2^k\right) - L_{\rho_1,\rho_2}\left(u^{k+1}, v^{k+1}, w^{k+1}, y^{k+1}, d_1^{k+1}, d_2^{k+1}\right) \\
\geq\ &\frac{1}{2\alpha}\|u^{k+1} - u^k\|^2 + \frac{1}{2}\|u^{k+1} - u^k\|_P^2 + \frac{\lambda_1 + \rho_1 c^2}{2}\|v^{k+1} - v^k\|^2 \\
&+ C_1\|w^{k+1} - w^k\|^2 + C_2\|y^{k+1} - y^k\|^2,
\end{aligned} \tag{3.12}$$

where

$$C_1 = \frac{\rho_1\epsilon^2}{2} - \frac{\lambda_2^2}{\rho_1 c^4}, \quad C_2 = \frac{\rho_2}{2} - \frac{L_\varphi^2}{\rho_2}, \quad P = \frac{1}{\alpha}I - \rho_1 H^\top H - \rho_2 L^\top L.$$

Proof. For the u-subproblem, based on Lemma 3.2, we derive

$$\begin{aligned} & L_{\rho_1,\rho_2}\big(u^k, v^k, w^k, y^k, d_1^k, d_2^k\big) - L_{\rho_1,\rho_2}\big(u^{k+1}, v^k, w^k, y^k, d_1^k, d_2^k\big) \\ \geq\ & \frac{1}{2\alpha}\|u^{k+1}-u^k\|^2 + \frac{1}{2}\|u^{k+1}-u^k\|_P^2. \end{aligned} \tag{3.13}$$

Similarly, for the v-subproblem, we obtain

$$\begin{aligned} & L_{\rho_1,\rho_2}\big(u^{k+1}, v^k, w^k, y^k, d_1^k, d_2^k\big) - L_{\rho_1,\rho_2}\big(u^{k+1}, v^{k+1}, w^k, y^k, d_1^k, d_2^k\big) \\ \geq\ & \frac{\lambda_1}{2}\|v^{k+1}-v^k\|^2 + \frac{\rho_1}{2}\|w^k\cdot(v^{k+1}-v^k)\|^2 \\ \geq\ & \frac{\lambda_1}{2}\|v^{k+1}-v^k\|^2 + \frac{\rho_1 c^2}{2}\|v^{k+1}-v^k\|^2 \\ =\ & \frac{\lambda_1+\rho_1 c^2}{2}\|v^{k+1}-v^k\|^2, \end{aligned} \tag{3.14}$$

where the second inequality results from $w_i^k \geq c > 0, \forall\, i$.

For the w-subproblem, we have

$$\begin{aligned} & L_{\rho_1,\rho_2}\big(u^{k+1}, v^{k+1}, w^k, y^k, d_1^k, d_2^k\big) - L_{\rho_1,\rho_2}\big(u^{k+1}, v^{k+1}, w^{k+1}, y^k, d_1^k, d_2^k\big) \\ \geq\ & \frac{\rho_1}{2}\|v^{k+1}\cdot(w^{k+1}-w^k)\|^2 \geq \frac{\rho_1\epsilon^2}{2}\|w^{k+1}-w^k\|^2, \end{aligned} \tag{3.15}$$

where the second inequality stems from $v_i^k \geq \epsilon > 0$ for any i.

Finally, for the y-subproblem, we obtain

$$\begin{aligned} & L_{\rho_1,\rho_2}\big(u^{k+1}, v^{k+1}, w^{k+1}, y^k, d_1^k, d_2^k\big) - L_{\rho_1,\rho_2}\big(u^{k+1}, v^{k+1}, w^{k+1}, y^{k+1}, d_1^k, d_2^k\big) \\ \geq\ & \frac{\rho_2}{2}\|y^{k+1}-y^k\|^2. \end{aligned} \tag{3.16}$$

From Lemma 3.3, it follows that

$$\begin{aligned} & L_{\rho_1,\rho_2}\big(u^{k+1}, v^{k+1}, w^{k+1}, y^{k+1}, d_1^k, d_2^k\big) - L_{\rho_1,\rho_2}\big(u^{k+1}, v^{k+1}, w^{k+1}, y^{k+1}, d_1^{k+1}, d_2^k\big) \\ =\ & -\frac{1}{\rho_1}\big\|d_1^{k+1}-d_1^k\big\|^2 \geq -\frac{\lambda_2^2}{\rho_1 c^4}\|w^{k+1}-w^k\|^2, \end{aligned} \tag{3.17}$$

$$\begin{aligned} & L_{\rho_1,\rho_2}\big(u^{k+1}, v^{k+1}, w^{k+1}, y^{k+1}, d_1^{k+1}, d_2^k\big) - L_{\rho_1,\rho_2}\big(u^{k+1}, v^{k+1}, w^{k+1}, y^{k+1}, d_1^{k+1}, d_2^{k+1}\big) \\ =\ & -\frac{1}{\rho_2}\big\|d_2^{k+1}-d_2^k\big\|^2 \geq -\frac{L_\varphi^2}{\rho_2}\|y^{k+1}-y^k\|^2. \end{aligned} \tag{3.18}$$

Because $\rho_1 > \sqrt{2}\lambda_2/(\epsilon c^2)$ and $\rho_2 > \sqrt{2}L_\varphi$, by adding (3.13)-(3.18), we can obtain (3.12), which completes the proof. □

Lemma 3.5. *We define $G : \Omega \to R$ as*

$$\begin{aligned} G(u,v,w,y) =\ & \frac{\lambda_1}{2}\|f-v\|^2 + \lambda_2\sum_i(w_i\cdot v_i - v_i - v_i\cdot\ln w_i) + \varphi(Lu) \\ & - \frac{\lambda_2^2}{2}\sum_i\left(1-\frac{1}{w_i}\right)^2 + \frac{\rho_1-1}{2}\|Hu-w\cdot v\|^2 + \frac{\rho_2-L_\varphi}{2}\|Lu-y\|^2, \end{aligned}$$

where $\rho_1 > 1, \rho_2 > L_\varphi$, and

$$\Omega = \big\{(u, v, w, y)|v_i \geq \epsilon > 0,\ w_i \geq c > 0,\ \forall\, i;\ \bar{c}^2\|u\|^2 \leq \|Hu\|^2 + \|Lu\|^2;\ u, v, w, y \in R^n\big\},$$

if

$$\|(u, v, w, y)\|_\Omega = \max\{\|u\|_\infty, \|v\|_\infty, \|w\|_\infty, \|y\|_\infty\} \ \rightarrow\ \infty,$$

then, under Assumption 3.2*, we have* $G(u, v, w, y) \to \infty$.

Proof. Let $(u, v, w, y) \in \Omega$, then we have the following estimation:

$$\begin{aligned} G(u, v, w, y) \geq\ & \frac{\lambda_1}{2}\|f - v\|^2 + \lambda_2\sum_i(w_i \cdot v_i - v_i - v_i \cdot w_i) + \varphi(Lu) - \frac{\lambda_2^2}{2}\sum_i\left(1 - \frac{1}{w_i}\right)^2 \\ & + \frac{\rho_1 - 1}{2}\|Hu - w \cdot v\|^2 + \frac{\rho_2 - L_\varphi}{2}\|Lu - y\|^2 \\ =\ & \frac{\lambda_1}{2}\|f - v\|^2 - \lambda_2\sum_i v_i + \varphi(Lu) - \frac{\lambda_2^2}{2}\sum_i\left(1 - \frac{1}{w_i}\right)^2 \\ & + \frac{\rho_1 - 1}{2}\|Hu - w \cdot v\|^2 + \frac{\rho_2 - L_\varphi}{2}\|Lu - y\|^2, \end{aligned}$$

where the first inequality holds because $-\ln w_i \geq -w_i$ if $w_i > 0$. It should be noted that $w_i \geq c > 0$ and $1 - 1/w_i \in [1 - 1/c, 1)$, and $(1 - 1/w_i)^2$ is bounded.

We now discuss four cases wherein $\{\|u\|_\infty, \|v\|_\infty, \|w\|_\infty, \|y\|_\infty\} \to \infty$.

Case 1. $\|v\|_\infty \to \infty$; it is clear that $G(u, v, w, y) \to \infty$.

Case 2. There exists a constant c_1 such that $\|v\|_\infty < c_1$ and $\|w\|_\infty \to \infty$. We obtain the following estimation:

$$\begin{aligned} G(u, v, w, y) &\geq \lambda_2\sum_i(w_i - 1) \cdot v_i - \lambda_2\sum_i v_i \ln w_i - \frac{\lambda_2^2}{2}\sum_i\left(1 - \frac{1}{w_i}\right)^2 \\ &\geq \lambda_2\epsilon\sum_i(w_i - 1) - \lambda_2 c_1\sum_i \ln w_i - \frac{\lambda_2^2}{2}\sum_i\left(1 - \frac{1}{w_i}\right)^2. \end{aligned}$$

Because

$$\lim_{w_i \to \infty} \frac{\lambda_2\epsilon(w_i - 1) - \lambda_2 c_1 \ln w_i - \lambda_2^2(1 - 1/w_i)^2/2}{w_i} = \lambda_2\epsilon > 0,$$

we can estimate

$$\left(\lambda_2\epsilon\sum_i(w_i - 1) - \lambda_2 c_1\sum_i \ln w_i - \frac{\lambda_2^2}{2}\sum_i\left(1 - \frac{1}{w_i}\right)^2\right) \ \rightarrow\ \infty \quad \text{as} \quad \|w\|_\infty \ \rightarrow\ \infty.$$

Therefore, we obtain $G(u, v, w, y) \to \infty$.

Case 3. Two constants c_2, c_3 exist such that $\|v\|_\infty < c_2, \|w\|_\infty < c_3$, and $\|u\|_\infty \to \infty$. It is known that $\bar{c}^2\|u\|^2 \leq \|Hu\|^2 + \|Lu\|^2 \to \infty$; therefore, $\|Hu\|_\infty \to \infty$ or $\|Lu\|_\infty \to \infty$. Under Assumption 3.2, we can easily obtain $G(u, v, w, y) \to \infty$.

Case 4. Three constants c_4, c_5, c_6 exist such that $\|v\|_\infty < c_4, \|w\|_\infty < c_5, \|u\|_\infty < c_6$, and $\|y\|_\infty \to \infty$. Because $\rho_2 > L_\varphi$, we can derive $G(u, v, w, y) \to \infty$.

In summary, we conclude that $G(u, v, w, y) \to \infty$ as $\|(u, v, w, y)\|_\Omega \to \infty$. □

Theorem 3.1. *Suppose that Assumptions* 3.1 *and* 3.2 *hold. Let* $\{(w^{k+1}, y^{k+1}, d_1^{k+1}, d_2^{k+1})\}$ *be the sequences generated by Algorithm* 3.1*, and let the iterative sequence* $\{w^k\}$ *has a uniformly positive lower bound. Let* $1 > \alpha(\rho_1\|H\|^2 + \rho_2\|L\|^2), \rho_1 > \max(\sqrt{2}\lambda_2/(\epsilon c^2), 1)$ *and* $\rho_2 > \sqrt{2}L_\varphi$*. Then, the following statements hold:*

(i) Sequence $(u^k, v^k, w^k, y^k, d_1^k, d_2^k)$ *generated by Algorithm* 3.1 *is bounded and has at least one limit point.*

(ii) Successive errors $u^{k+1} - u^k \to 0, v^{k+1} - v^k \to 0, w^{k+1} - w^k \to 0, y^{k+1} - y^k \to 0$ *and* $d_1^{k+1} - d_1^k \to 0, d_2^{k+1} - d_2^k \to 0$.

(iii) Each limit point $(u^*, v^*, w^*, y^*, d_1^*, d_2^*)$ *is a stationary point of* $L_{\rho_1,\rho_2}(u, v, w, y, d_1, d_2)$.

Proof. (i) From Lemma 3.4, we know that $L_{\rho_1,\rho_2}(u^k, v^k, w^k, y^k, d_1^k, d_2^k)$ is monotonically decreasing. Next, we prove that $L_{\rho_1,\rho_2}(u^k, v^k, w^k, y^k, d_1^k, d_2^k)$ has a lower bound.

It can be easily interpreted that

$$
\begin{aligned}
&L_{\rho_1,\rho_2}(u^k, v^k, w^k, y^k, d_1^k, d_2^k)\\
\geq\ &\frac{\lambda_1}{2}\|f - v^k\|^2 + \lambda_2\sum_i\left(w_i^k \cdot v_i^k - v_i^k - v_i^k \cdot \ln w_i^k\right) + \varphi(y^k) - \frac{\lambda_2^2}{2}\sum_i\left(1 - \frac{1}{w_i^k}\right)^2\\
&+ \frac{\rho_1 - 1}{2}\|Hu^k - w^k \cdot v^k\|^2 + \left\langle d_2^k, Lu^k - y^k\right\rangle + \frac{\rho_2}{2}\|Lu^k - y^k\|^2\\
\geq\ &\frac{\lambda_1}{2}\|f - v^k\|^2 + \lambda_2\sum_i\left(w_i^k \cdot v_i^k - v_i^k - v_i^k \cdot \ln w_i^k\right) + \varphi(y^k) - \frac{\lambda_2^2}{2}\sum_i\left(1 - \frac{1}{w_i^k}\right)^2\\
&+ \frac{\rho_1 - 1}{2}\|Hu^k - w^k \cdot v^k\|^2 + \langle\nabla\varphi(y^k), Lu^k - y^k\rangle\\
&+ \frac{\rho_2 - L_\varphi}{2}\|Lu^k - y^k\|^2 + \frac{L_\varphi}{2}\|Lu^k - y^k\|^2\\
\geq\ &\frac{\lambda_1}{2}\|f - v^k\|^2 + \lambda_2\sum_i\left(w_i^k \cdot v_i^k - v_i^k - v_i^k \cdot \ln w_i^k\right) + \varphi(Lu^k) - \frac{\lambda_2^2}{2}\sum_i\left(1 - \frac{1}{w_i^k}\right)^2\\
&+ \frac{\rho_1 - 1}{2}\|Hu^k - w^k \cdot v^k\|^2 + \frac{\rho_2 - L_\varphi}{2}\|Lu^k - y^k\|^2\\
=\ &G(u^k, v^k, w^k, y^k).
\end{aligned}
\tag{3.19}
$$

Thus, combined with Lemma 3.5 and (3.19), the sequences $\{u^k\}, \{v^k\}, \{w^k\}, \{y^k\}$, and $G(u^k, v^k, w^k, y^k)$ are all bounded, and the boundedness of $\{d_1^k\}, \{d_2^k\}$ is due to Lemma 3.1, and $\nabla\varphi(y^k)=d_2^k$.

Owing to the boundedness of sequence $(u^k, v^k, w^k, y^k, d_1^k, d_2^k)$, there must be a convergent subsequence $(u^{k_i}, v^{k_i}, w^{k_i}, y^{k_i}, d_1^{k_i}, d_2^{k_i})$, i.e. $(u^{k_i}, v^{k_i}, w^{k_i}, y^{k_i}, d_1^{k_i}, d_2^{k_i}) \to (u^*, v^*, w^*, y^*, d_1^*, d_2^*)$.

(ii) From (3.19), it is evident that sequence $L_{\rho_1,\rho_2}(u^k, v^k, w^k, y^k, d_1^k, d_2^k)$ is also bounded. By summing (3.12) from $k = 1$ to ∞, we obtain

$$
\sum_{k=1}^{\infty}\left(\|u^{k+1} - u^k\|^2 + \|v^{k+1} - v^k\|^2 + \|w^{k+1} - w^k\|^2 + \|y^{k+1} - y^k\|^2\right) < \infty.
$$

Therefore, we obtain $u^{k+1} - u^k \to 0, v^{k+1} - v^k \to 0, w^{k+1} - w^k \to 0, y^{k+1} - y^k \to 0$. From Lemma 3.3, we can also obtain $d_1^{k+1} - d_1^k \to 0, d_2^{k+1} - d_2^k \to 0$.

(iii) According to the optimality condition of the u-subproblem, we deduce that there exists $q_1 \in \partial\delta_U(u^{k+1})$ such that

$$\begin{aligned}&q_1 + H^\top d_1^k + \rho_1 H^\top (Hu^{k+1} - w^k \cdot v^k)\\&\quad + L^\top d_2^k + \rho_2 L^\top (Lu^{k+1} - y^k) + P(u^{k+1} - u^k) = 0.\end{aligned}$$

Let

$$\begin{aligned}p_1 &= q_1 + H^\top d_1^{k+1} + \rho_1 H^\top (Hu^{k+1} - w^{k+1} \cdot v^{k+1})\\&\quad + L^\top d_2^{k+1} + \rho_2 L^\top (Lu^{k+1} - y^{k+1})\\&\in \partial_u L_{\rho_1,\rho_2}\big(u^{k+1}, v^{k+1}, w^{k+1}, y^{k+1}, d_1^{k+1}, d_2^{k+1}\big),\end{aligned}$$

then, we have

$$\begin{aligned}\|p_1\| &= \big\|q_1 + H^\top d_1^{k+1} + \rho_1 H^\top (Hu^{k+1} - w^{k+1} \cdot v^{k+1}) + L^\top d_2^{k+1} + \rho_2 L^\top (Lu^{k+1} - y^{k+1})\big\|\\&= \big\|H^\top \big(d_1^{k+1} - d_1^k\big) + \rho_1 H^\top (w^k \cdot v^k - w^{k+1} \cdot v^{k+1}) + L^\top \big(d_2^{k+1} - d_2^k\big)\\&\quad + \rho_2 L^\top (y^k - y^{k+1}) - P(u^{k+1} - u^k)\big\|\\&= \big\|H^\top \big(d_1^{k+1} - d_1^k\big) + \rho_1 H^\top \big[- w^k \cdot (v^{k+1} - v^k) - v^{k+1} \cdot (w^{k+1} - w^k)\big]\\&\quad + L^\top \big(d_2^{k+1} - d_2^k\big) + \rho_2 L^\top (y^k - y^{k+1}) - P(u^{k+1} - u^k)\big\|\\&\le \big\|H^\top \big(d_1^{k+1} - d_1^k\big)\big\| + \rho_1 \|H^\top w^k \cdot (v^{k+1} - v^k)\| + \rho_1 \|H^\top v^{k+1} \cdot (w^{k+1} - w^k)\|\\&\quad + \big\|L^\top \big(d_2^{k+1} - d_2^k\big)\big\| + \rho_2 \|L^\top (y^{k+1} - y^k)\| + \|P(u^{k+1} - u^k)\|.\end{aligned} \tag{3.20}$$

The optimality condition of the v-subproblem implies that there exists $q_2 \in \partial \delta_V(v^{k+1})$ such that

$$\begin{aligned}0 &= q_2 + \lambda_2 (w^k - I - \ln w^k) - \lambda_1 (f - v^{k+1}) - \rho_1 w^k \cdot (Hu^{k+1} - w^k \cdot v^{k+1}) - w^k \cdot d_1^k\\&= q_2 - \lambda_2 \ln w^k + \lambda_1 v^{k+1} - \lambda_1 f + \rho_1 (w^k)^2 \cdot v^{k+1} - \rho_1 w^k \cdot Hu^{k+1},\end{aligned}$$

where the second equal sign results from Lemma 3.1.

Let

$$\begin{aligned}p_2 &= q_2 + \lambda_2 (w^{k+1} - I - \ln w^{k+1}) - \lambda_1 (f - v^{k+1})\\&\quad - \rho_1 w^{k+1} \cdot (Hu^{k+1} - w^{k+1} \cdot v^{k+1}) - w^{k+1} \cdot d_1^{k+1}\\&\in \partial_v L_{\rho_1,\rho_2}\big(u^{k+1}, v^{k+1}, w^{k+1}, y^{k+1}, d_1^{k+1}, d_2^{k+1}\big),\end{aligned}$$

then we obtain

$$\begin{aligned}\|p_2\| &= \big\|q_2 + \lambda_2 (w^{k+1} - I - \ln w^{k+1}) - \lambda_1 (f - v^{k+1}) - w^{k+1} \cdot d_1^{k+1}\\&\quad - \rho_1 w^{k+1} \cdot (Hu^{k+1} - w^{k+1} \cdot v^{k+1})\big\|\\&= \big\|\rho_1 v^{k+1} \cdot \big[(w^{k+1})^2 - (w^k)^2\big] + \lambda_2 (\ln w^k - \ln w^{k+1})\\&\quad - \rho_1 Hu^{k+1} \cdot (w^{k+1} - w^k)\big\|\\&= \big\|\big[\rho_1 v^{k+1} \cdot (w^{k+1} + w^k) - \rho_1 Hu^{k+1}\big] \cdot (w^{k+1} - w^k)\\&\quad + \lambda_2 (\ln w^k - \ln w^{k+1})\big\|\\&= \big\|\big(d_1^k - d_1^{k+1}\big) \cdot (w^{k+1} - w^k) + \rho_1 v^{k+1} \cdot w^k \cdot (w^{k+1} - w^k)\\&\quad + \lambda_2 (\ln w^k - \ln w^{k+1})\big\|\\&\le \big\|d_1^{k+1} - d_1^k\big\| \, \|w^{k+1} - w^k\| + \rho_1 \|v^{k+1} \cdot w^k \cdot (w^{k+1} - w^k)\|\\&\quad + \lambda_2 \|\ln w^{k+1} - \ln w^k\|.\end{aligned} \tag{3.21}$$

From the optimality condition of the w-subproblem and Lemma 3.1, we obtain

$$\begin{aligned}
&\left\|\nabla_w L_{\rho_1,\rho_2}\left(u^{k+1}, v^{k+1}, w^{k+1}, y^{k+1}, d_1^{k+1}, d_2^{k+1}\right)\right\| \\
={}& \left\|\lambda_2(w^{k+1}\cdot v^{k+1} - v^{k+1}) - \rho_1 v^{k+1}\cdot w^{k+1}\cdot\left(Hu^{k+1} - w^{k+1}\cdot v^{k+1} + \frac{d_1^{k+1}}{\rho_1}\right)\right\| \\
={}& \left\|\rho_1(v^{k+1})^2\cdot(w^{k+1})^2 + \left(\lambda_2 v^{k+1} - \rho_1 v^{k+1}\cdot Hu^{k+1} - v^{k+1}\cdot d_1^{k+1}\right)\cdot w^{k+1} - \lambda_2 v^{k+1}\right\| \\
={}& \left\|\rho_1(v^{k+1})^2\cdot(w^{k+1})^2 + \left(\lambda_2 v^{k+1} - \rho_1 v^{k+1}\cdot Hu^{k+1} - v^{k+1}\cdot d_1^{k+1}\right)\cdot w^{k+1}\right. \\
&\quad \left. - \left(\lambda_2 w^{k+1} - w^{k+1}\cdot d_1^{k+1}\right)\cdot v^{k+1}\right\| \\
={}& \left\|v^{k+1}\cdot w^{k+1}\cdot\left(\rho_1 v^{k+1}\cdot w^{k+1} + \lambda_2 - \rho_1 Hu^{k+1} - d_1^{k+1} - \lambda_2 + d_1^{k+1}\right)\right\| \\
={}& \left\|v^{k+1}\cdot w^{k+1}\cdot\left(d_1^k - d_1^{k+1}\right)\right\|. \qquad (3.22)
\end{aligned}$$

The optimality condition of the y-subproblem and the update rule of the multipliers d_1^{k+1}, d_2^{k+1} yield

$$\begin{aligned}
&\left\|\nabla_y L_{\rho_1,\rho_2}\left(u^{k+1}, v^{k+1}, w^{k+1}, y^{k+1}, d_1^{k+1}, d_2^{k+1}\right)\right\| \\
={}& \left\|\nabla\varphi(y^{k+1}) - d_2^{k+1} - \rho_2(Lu^{k+1} - y^{k+1})\right\| = \left\|d_2^k - d_2^{k+1}\right\|, \qquad (3.23) \\
&\left\|\nabla_{d_1} L_{\rho_1,\rho_2}\left(u^{k+1}, v^{k+1}, w^{k+1}, y^{k+1}, d_1^{k+1}, d_2^{k+1}\right)\right\| \\
={}& \left\|Hu^{k+1} - w^{k+1}\cdot v^{k+1}\right\| = \frac{1}{\rho_1}\left\|d_1^{k+1} - d_1^k\right\|, \qquad (3.24) \\
&\left\|\nabla_{d_2} L_{\rho_1,\rho_2}\left(u^{k+1}, v^{k+1}, w^{k+1}, y^{k+1}, d_1^{k+1}, d_2^{k+1}\right)\right\| \\
={}& \left\|Lu^{k+1} - y^{k+1}\right\| = \frac{1}{\rho_2}\left\|d_2^{k+1} - d_2^k\right\|. \qquad (3.25)
\end{aligned}$$

Therefore, by combining (ii) and (3.20)-(3.25), we conclude that $(u^*, v^*, w^*, y^*, d_1^*, d_2^*)$ is a stationary point of $L_{\rho_1,\rho_2}(u, v, w, y, d_1, d_2)$. □

4. Numerical Experiments

In this section, we discuss a few numerical experiments to illustrate the performance of the proposed algorithm (Algorithm 3.1) on the mixed Poisson-Gaussian noise removal problem. All experiments were performed on a 64-bit Windows 10 operating system with an Intel Pentium G4400 CPU and 4 GB memory. All the source code was tested using MATLAB R2020b. The source code used in this paper can be downloaded at `https://github.com/hhaaoo1331/Mixed-Poisson-Gaussian`.

We used the peak signal-to-noise ratio (PSNR) and structural similarity (SSIM) [37] to evaluate the quality of the restored images. They are defined as follows:

$$\mathrm{PSNR} = 10\log_{10}\left(\frac{MN|u_{\max} - u_{\min}|^2}{\|u - \tilde{u}\|^2}\right),$$

where u is the original image, $\tilde{u}$ denotes the recovered image, $u_{\max}$ and $u_{\min}$ represent the maximum and minimum pixel values, respectively, and M and N indicate the image sizes.

$$\mathrm{SSIM} = \frac{(2\mu_u\mu_{\tilde{u}} + C_1)(2\sigma_{u\tilde{u}} + C_2)}{\left(\mu_u^2 + \mu_{\tilde{u}}^2 + C_1\right)\left(\sigma_u^2 + \sigma_{\tilde{u}}^2 + C_2\right)},$$

where μ_u and $\mu_{\tilde{u}}$ represent the averages of u and $\tilde{u}$, respectively, σ_u^2 and $\sigma_{\tilde{u}}^2$ are the corresponding variances, $\sigma_{u\tilde{u}}$ represents the corresponding covariance, and C_1 and C_2 represent the two fixed variables. The stopping criterion used in all experiments is defined as

$$\frac{\|u^{k+1} - u^k\|}{\|u^k\|} \leq 10^{-4},$$

or the maximum number of iterations becomes 1000.

We selected three images for testing, which are illustrated in Fig. 4.1. We first scaled the pixel value of the test image u, that is, the pixel value was adjusted from the original $[0, 255]$ to $[0, 1]$. We considered different blur kernels H (H_1: Gaussian blur (`fspecial ("Gaussian," [7,7], 3)`); H_2: Disk blur (`fspecial ("disk," 3)`)) to obtain a blurred image $g = Hu$, and then we used `Poissrnd` $(\eta g)/\eta$ to add Poisson noise, where η represents the scale factor used to control the size of the Poisson noise. Further, additive Gaussian noise with mean zero and standard variance σ was added to obtain the final observed noise image, f. In the experiment, we selected three different Poisson noise levels and two different Gaussian noise variances for testing, namely, $\eta = 1, 4, 16$ and $\sigma = 10^{-1}, 10^{-2}$.

We used $\varphi(Lu) = \sum_{i,j} |(Lu)_{i,j}|_\gamma$ (Huber-TV) as the regularization function, where

$$|z|_\gamma = \begin{cases} |z| - \dfrac{\gamma}{2}, & \text{if} \quad |z| \geq \gamma \\ \dfrac{1}{2\gamma}|z|^2, & \text{if} \quad |z| < \gamma. \end{cases} \tag{4.1}$$

In particular, when $\gamma = 0$, the Huber-TV coincides with the standard TV regularization. Herein, we will refer to the corresponding algorithm as PBCA+Huber. In contrast, we will refer to the PBCA algorithm that directly uses the TV regularization as PBCA+TV. Although the corresponding iterative algorithm is not guaranteed to converge, it achieves satisfactory performance in practice.

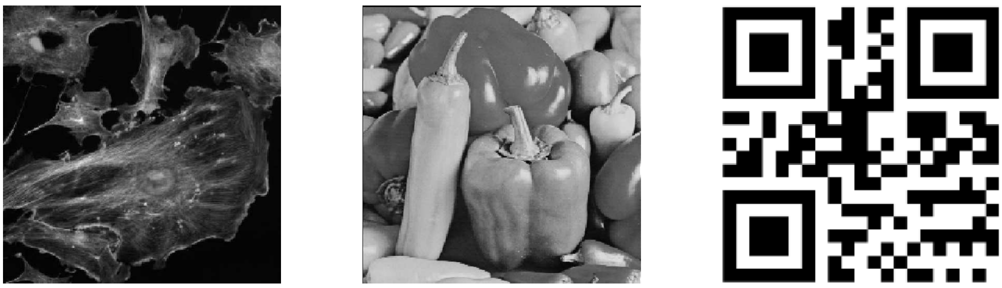

(a) (b) (c)

Fig. 4.1. (a) 256×256 "Fluorescent Cells"; (b) 256×256 "Peppers"; (c) 256×256 "Two Code".

4.1. Parameter discussion

In this subsection, we evaluate the influence of parameters $\gamma, \rho_1, \rho_2, \epsilon$, and α in the context of the PBCA+Huber algorithm. We chose "Fluorescent Cells" as the test image, and the noise level was set to $\eta = 16, \sigma = 10^{-1}$, with H as Gaussian blur (`fspecial ("Gaussian," [7,7], 3)`). In Fig. 4.2, we demonstrate the effect of parameter ρ_1 from 10 to 5000 on the PBCA+Huber algorithm by plotting the change in PSNR. However, it should be noted that

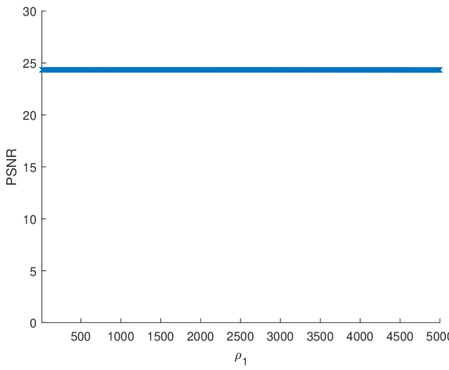

(a) ρ_1

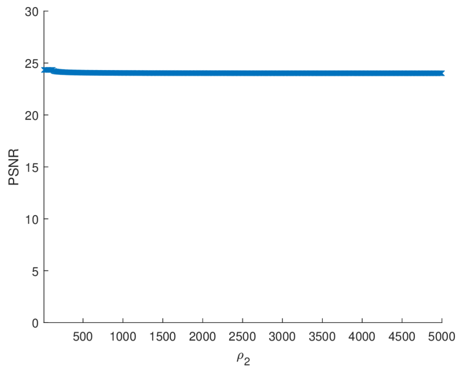

(b) ρ_2

Fig. 4.2. Change in PSNR with respect to parameters ρ_1 and ρ_2 for the PBCA+Huber algorithm.

the other parameters γ, ρ_2, ϵ, and α are fixed. We can infer that parameter ρ_1 has little effect on the algorithm. Similarly, we present the effect of parameter ρ_2 from 10 to 5000 on the PBCA+Huber algorithm, where the other parameters γ, ρ_1, ϵ, and α are fixed. Evidently, the PSNR values decrease slightly when parameter $\rho_2 > 120$.

For parameter γ in Huber-TV, if γ tends to 0, the Huber-TV regularization function approximately equals to the TV regularization function. Therefore, we fixed parameters ρ_1, ρ_2, ϵ, and α and changed γ from 10^{-5} to 10^{-1}. We plot the changes in PSNR values in Fig. 4.3. It can be observed that the PSNR values remain nearly unchanged when γ lies in the range of 10^{-2} to 6×10^{-2}.

An extremely small positive scale factor ϵ must be introduced to prove the convergence of the PBCA algorithm; therefore, it is necessary to evaluate whether the value of ϵ affects the PBCA algorithm. To do so, we fixed ρ_1, ρ_2, γ, and α and changed ϵ from 10^{-10} to 10^{-1}. The result of the change in PSNR values is presented in Fig. 4.4. The results show that the PSNR values remain nearly unchanged when ϵ lies in the range of 10^{-10} to 5×10^{-2}.

For parameter α in the positive definite matrix P, when the value of α is large, the matrix P may not be positive definite, leading to poor experimental results. Therefore, we fixed $\gamma, \rho_1, \rho_2, \epsilon$ and varied α from 10^{-5} to 10^{-2}; the corresponding change in PSNR values is shown in Fig. 4.5. It can be observed that when $\alpha < 1.5 \times 10^{-4}$, the algorithm converges slowly, and the PSNR

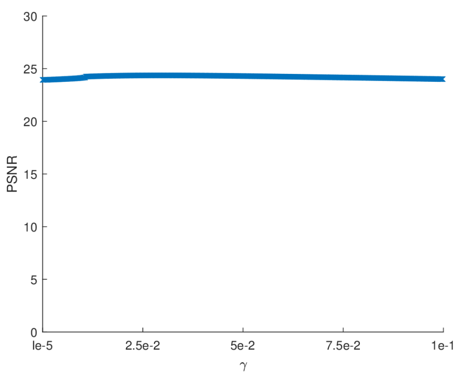

Fig. 4.3. Change in PSNR with respect to parameter γ for the PBCA+Huber algorithm.

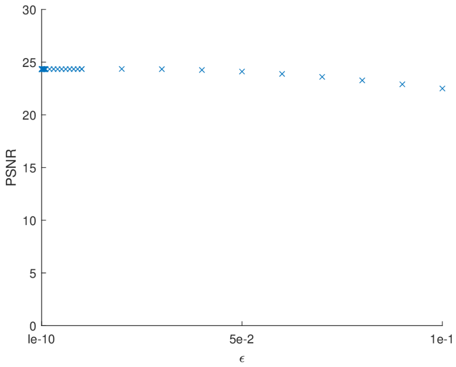

Fig. 4.4. Change in PSNR with respect to parameter ϵ for the PBCA+Huber algorithm.

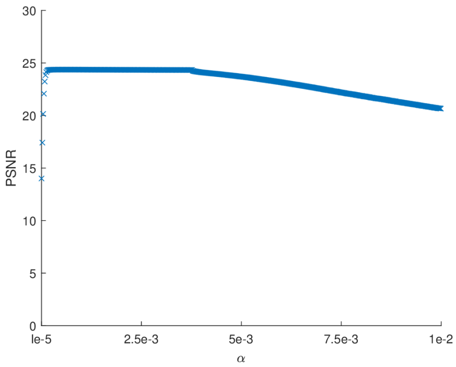

Fig. 4.5. Change in PSNR with respect to parameter α for the PBCA+Huber algorithm.

values are small. When $1.5 \times 10^{-4} \leq \alpha \leq 4 \times 10^{-3}$, the PSNR values remain almost unchanged. When $\alpha > 4 \times 10^{-3}$, the PSNR values begin to decrease continuously.

Therefore, in the subsequent experiments, we set $\gamma = 0.02, \rho_1 = 300, \rho_2 = 80, \epsilon = 10^{-5}$ and $\alpha = 0.003$.

4.2. Mixed Poisson-Gaussian deblurring

In this subsection, we present the results of some experiments with the PBCA algorithm for image deblurring under mixed Poisson-Gaussian noise. We compare the algorithm with other popular algorithms employed to solve the TV-IC model, including the primal-dual-based iterative algorithm (PD+TV) [17] and the primal-dual hybrid gradient algorithm (PDHG+TV) [35].

Regularization parameters, λ_1, and λ_2 were used to balance the data-fitting and regularization terms, which play an important role in the experimental results. Fig. 4.6 presents a three-dimensional relationship diagram of the regularization parameters, λ_1 and λ_2, and the PSNR values in the PBCA+Huber algorithm. We used this method to determine the optimal values of the regularization parameters, λ_1 and λ_2. Owing to space limitations, we directly provide the optimal regularization parameters, λ_1, and λ_2 of the PBCA algorithm under other noise levels in Table 4.1. In Table 4.2, we present the recovery results of PSNR and SSIM values for all the algorithms under different noise levels. Compared with other algorithms, our proposed PBCA algorithm achieves higher PSNR values. In Fig. 4.7, we present the restoration

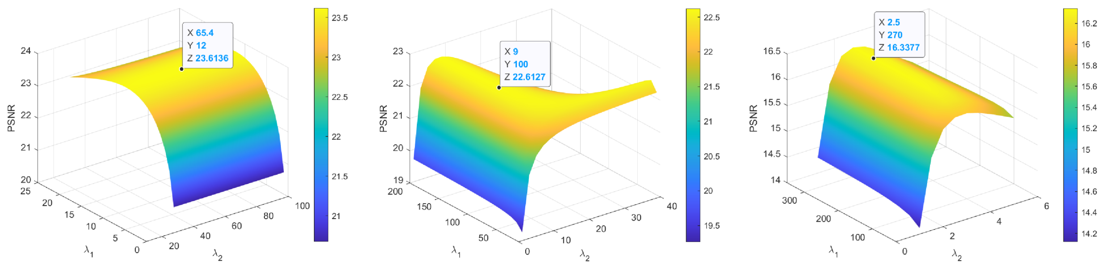

(a) (b) (c)

Fig. 4.6. Evolution of PSNR (dB) under different regularization parameters. Black dots represent the optimal PSNR value and the corresponding values of regularization parameters λ_1 and λ_2. (a): $\eta = 4$, $\sigma = 10^{-2}$, H = `fspecial ("disk," 3)`, the test image is “Fluorescent Cells”; (b): η=16, σ=10^{-1}, H = `fspecial ("disk," 3)`, the test image is “Peppers”; (c): $\eta = 1, \sigma = 10^{-2}$, H = `fspecial ("Gaussian," [7,7], 3)`, the test image is “Two Code”.

results for three test images with different noise levels. In Fig. 4.8, we present the changes in PSNR to the elapsed CPU time. The results show that the PBCA algorithm is faster than the PD+TV and PDHG+TV algorithms.

Table 4.1: Regularization parameter settings in mixed Poisson-Gaussian noise deblurring.

Image	η	H	Method	$\sigma = 10^{-1}$		$\sigma = 10^{-2}$	
				λ_1	λ_2	λ_1	λ_2
Fluorescent Cells	1	H_1	PBCA+TV	4.4	250	300	1.1
			PBCA+Huber	4.1	120	264.5	1.1
		H_2	PBCA+TV	4	77	112	1
			PBCA+Huber	3.8	72.1	122.3	1
	4	H_1	PBCA+TV	11.8	94	354	3.6
			PBCA+Huber	11.8	100	260	3.3
		H_2	PBCA+TV	9.6	285	12	78
			PBCA+Huber	9.4	220	12	65.4
	16	H_1	PBCA+TV	23.4	88	443.2	9
			PBCA+Huber	23.7	160	230	10
		H_2	PBCA+TV	23.8	88.4	449	8.2
			PBCA+Huber	23.2	86.7	230	9
Peppers	1	H_1	PBCA+TV	350	1.9	211.8	1.7
			PBCA+Huber	350	1.7	199.7	1.7
		H_2	PBCA+TV	469.6	2	180	1.6
			PBCA+Huber	349.8	1.6	170	1.5
	4	H_1	PBCA+TV	230	3.9	309	4.1
			PBCA+Huber	261	4.1	210	4.2
		H_2	PBCA+TV	498	3.8	280	3.7
			PBCA+Huber	110	3.9	110	4
	16	H_1	PBCA+TV	237	8.3	176	11.8
			PBCA+Huber	140	9.2	120	13.2
		H_2	PBCA+TV	274	8.1	448.4	9
			PBCA+Huber	100	9	300	9.5

Table 4.1: Regularization parameter settings in mixed Poisson-Gaussian noise deblurring (cont'd).

Image	η	H	Method	$\sigma = 10^{-1}$		$\sigma = 10^{-2}$	
				λ_1	λ_2	λ_1	λ_2
Two Code	1	H_1	PBCA+TV	61	2.2	210	2.4
			PBCA+Huber	64.1	2.7	270	2.5
		H_2	PBCA+TV	39.6	2.2	60	2.2
			PBCA+Huber	4.1	11.2	4.6	8
	4	H_1	PBCA+TV	141.2	6	1500	4.6
			PBCA+Huber	126.8	5.7	1300	5.2
		H_2	PBCA+TV	122	3.8	1350	4
			PBCA+Huber	135.5	5	1350	4.4
	16	H_1	PBCA+TV	158.6	9.6	2500	9
			PBCA+Huber	55	22.1	399.1	11.3
		H_2	PBCA+TV	125.2	8.6	1500	8.4
			PBCA+Huber	36	19.2	1300	9.2

Table 4.2: PSNR (dB) and SSIM of the compared methods for deblurring with mixed Poisson-Gaussian noise.

Image	η	σ	H	Input	PD+TV	PDHG+TV	PBCA+TV	PBCA+Huber
Fluorescent Cells	1	10^{-1}	H_1	6.95	22.00	21.81	21.87	**22.28**
				0.0411	0.4580	0.4495	0.4517	**0.4836**
			H_2	6.92	21.45	21.48	21.52	**21.83**
				0.0240	0.4283	0.4179	0.4225	**0.4566**
		10^{-2}	H_1	7.02	21.85	21.48	21.75	**22.09**
				0.0307	**0.4577**	0.4231	0.4096	0.4287
			H_2	7.09	21.88	21.33	21.82	**22.15**
				0.0360	**0.4563**	0.4011	0.4164	0.4328
	4	10^{-1}	H_1	12.18	23.03	22.80	22.84	**23.13**
				0.0571	0.5116	0.5007	0.5028	**0.5147**
			H_2	12.17	22.93	22.90	22.94	**23.33**
				0.0610	0.5038	0.5102	0.5116	**0.5291**
		10^{-2}	H_1	12.93	23.21	22.89	22.98	**23.35**
				0.0874	**0.5329**	0.4869	0.4912	0.5108
			H_2	13.00	23.22	23.25	23.29	**23.61**
				0.0950	0.5251	0.5299	0.5321	**0.5531**
	16	10^{-1}	H_1	16.07	23.87	23.67	23.72	**24.12**
				0.1138	0.5467	0.5487	0.5510	**0.5552**
			H_2	16.13	24.05	23.94	23.98	**24.34**
				0.1258	0.5541	0.5645	0.5661	**0.5729**
		10^{-2}	H_1	18.25	24.40	24.12	24.17	**24.63**
				0.2253	0.5932	0.5713	0.5738	**0.5935**
			H_2	18.32	24.50	24.40	24.45	**24.85**
				0.2399	0.5541	0.5943	0.5952	**0.6126**

Table 4.2: PSNR (dB) and SSIM of the compared methods for deblurring with mixed Poisson-Gaussian noise (cont'd).

Image	η	σ	H	Input	PD+TV	PDHG+TV	PBCA+TV	PBCA+Huber
Peppers	1	10^{-1}	H_1	3.08 0.0151	18.84 0.5198	18.93 0.5276	19.12 0.5274	**19.28** **0.5567**
			H_2	3.07 0.0163	19.09 0.5263	19.11 0.5368	19.15 0.5129	**19.46** **0.5608**
		10^{-2}	H_1	3.14 0.0162	18.74 0.5058	18.90 0.5102	19.14 0.5265	**19.26** **0.5418**
			H_2	3.13 0.0184	19.03 0.4898	19.23 0.5321	19.44 0.5423	**19.54** **0.5636**
	4	10^{-1}	H_1	8.67 0.0452	20.32 0.5633	20.66 0.6054	20.81 0.6113	**20.95** **0.6248**
			H_2	8.72 0.0526	20.67 0.5731	20.98 0.6252	21.16 0.6202	**21.31** **0.6437**
		10^{-2}	H_1	9.05 0.0483	20.45 0.5749	20.72 0.6036	20.92 0.6133	**21.06** **0.6320**
			H_2	9.02 0.0525	20.59 0.5589	20.93 0.6136	21.17 0.6186	**21.25** **0.6319**
	16	10^{-1}	H_1	13.48 0.1066	21.51 0.6127	21.80 0.6587	21.89 0.6624	**22.10** **0.6824**
			H_2	13.58 0.1153	21.92 0.6216	22.29 0.6781	22.40 0.6816	**22.61** **0.7015**
		10^{-2}	H_1	14.56 0.1331	21.85 0.6471	22.28 0.6761	22.35 0.6788	**22.60** **0.7070**
			H_2	14.65 0.1437	22.08 0.6423	22.55 0.6917	22.66 0.6971	**22.87** **0.7158**
Two Code	1	10^{-1}	H_1	2.21 0.0936	14.97 0.5480	15.13 0.5431	15.86 **0.5882**	**15.87** 0.5867
			H_2	2.25 0.1113	15.35 0.5586	15.62 0.5619	**16.41** **0.6019**	16.06 0.5882
		10^{-2}	H_1	2.27 0.1385	15.07 0.5864	15.21 0.5556	16.30 **0.7470**	**16.33** 0.7331
			H_2	2.38 0.1643	15.29 0.5866	15.38 0.5527	**16.19** **0.7224**	15.88 0.5918
	4	10^{-1}	H_1	7.45 0.1868	17.45 0.6478	18.21 0.6853	18.71 **0.6900**	**18.74** **0.6900**
			H_2	7.63 0.2186	18.24 0.6856	18.78 0.6985	19.32 **0.7095**	**19.35** 0.7021
		10^{-2}	H_1	17.65 0.2351	17.90 0.7218	18.47 0.6980	20.13 **0.8734**	**20.17** 0.8625
			H_2	7.88 0.2810	18.50 0.7262	19.11 0.7095	19.98 **0.8668**	**20.00** 0.8555
	16	10^{-1}	H_1	11.22 0.2739	20.12 0.7863	20.96 **0.8376**	21.19 0.7616	**21.41** 0.8177
			H_2	11.67 0.3130	20.81 0.7995	21.85 **0.8456**	21.96 0.7751	**22.25** 0.8282
		10^{-2}	H_1	11.81 0.3336	21.05 0.8716	21.59 0.8680	**24.08** **0.9365**	23.67 0.9247
			H_2	12.40 0.3975	22.00 0.9074	22.59 0.8657	23.98 **0.9370**	**24.01** 0.9268

(a) Input:16.13 (b) Input:14.56 (c) Input:12.40

(d) PD+TV:24.05 (e) PD+TV:21.85 (f) PD+TV:22.00

(g) PDHG+TV:23.94 (h) PDHG+TV:22.28 (i) PDHG+TV:22.59

(j) PBCA+TV:23.98 (k) PBCA+TV:22.35 (l) PBCA+TV:23.98

(m) PBCA+Huber:24.34 (n) PBCA+Huber:22.60 (o) PBCA+Huber:24.01

Fig. 4.7. Results of different algorithms (with PSNR(dB) below the figures) for mixed Poisson-Gaussian noise deblurring. (a): "Fluorescent Cells", noise level: $\eta = 16, \sigma = 10^{-1}$, H `= fspecial (\disk," 3)`; (b): "Peppers", noise level: $\eta = 16, \sigma = 10^{-2}$, H `= fspecial (\Gaussian," [7,7], 3)`; (c): "Two Code", noise level: $\eta = 16, \sigma = 10^{-2}$, H `= fspecial (\disk," 3)`.

To demonstrate the convergence of the PBCA+TV and PBCA+Huber algorithms, the PSNR values are plotted with the number of iterations in Fig. 4.9. It can be observed that the final PSNR values remain unchanged. Therefore, we can conclude that the proposed algorithm is convergent.

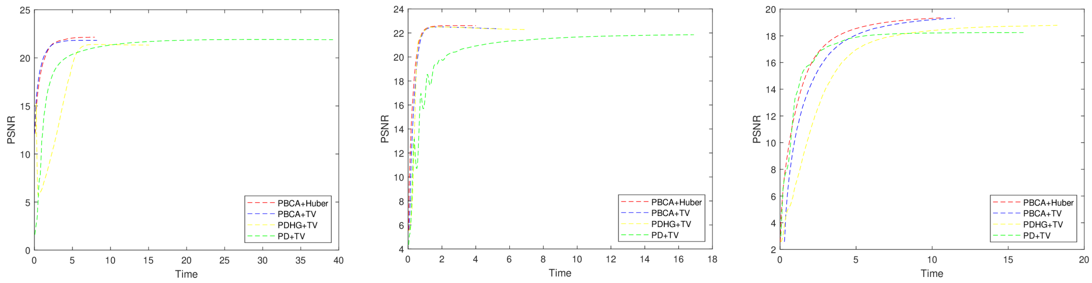

Fig. 4.8. PSNR(dB) versus CPU time (in seconds) for algorithms: PBCA+Huber, PBCA+TV, PDHG+TV, and PD+TV for mixed Poisson-Gaussian noise deblurring. Left: $\eta = 1, \sigma = 10^{-2}$, H `= fspecial ("disk," 3)`, the test image is “Fluorescent Cells”; Middle: $\eta = 16, \sigma = 10^{-2}$, H `= fspecial ("Gaussian," [7,7], 3)`, the test image is “Peppers”; Right: $\eta = 4, \sigma = 10^{-1}$, H `= fspecial ("disk," 3)`, the test image is “Two Code”.

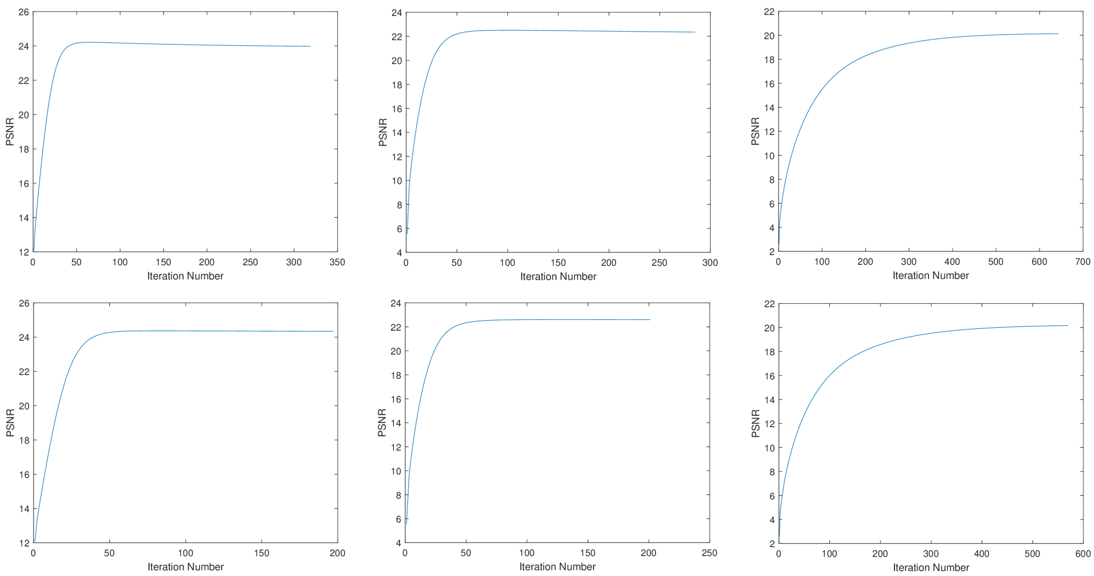

Fig. 4.9. PSNR(dB) versus number of iterations: Top: PBCA+TV; Bottom: PBCA+Huber; Left: $\eta = 16, \sigma = 10^{-1}$, H `= fspecial ("disk," 3)`, the test image is “Fluorescent Cells”; Middle: η=16, $\sigma = 10^{-2}$, H `= fspecial ("Gaussian," [7,7], 3)`, the test image is “Peppers”; Right: $\eta = 4, \sigma = 10^{-2}$, H `= fspecial ("Gaussian," [7,7], 3)`, the test image is “Two Code”.

4.3. Mixed Poisson-Gaussian denoising

In this subsection, we present some experimental results of the PBCA algorithm for pure denoising under mixed Poisson-Gaussian noise and compare them with those of the BCA [40] algorithm. The selection of the Poisson noise scale factor η and Gaussian noise variance σ is the same as described above.

Table 4.3 provides the optimal values of regularization parameters λ_1 and λ_2 for the PBCA algorithm for different noise levels. In Fig. 4.10, the recovery result of "Fluorescent Cells" indicates that the performance of the PBCA+Huber algorithm is almost the same as that of the BCA algorithm. The recovery results of "Peppers" and "Two Code" show that our method exhibits higher PSNR values than all other methods. In Table 4.4, we present the numerical results of the PSNR and SSIM values for all the algorithms at different levels of noise.

Table 4.3: Regularization parameter settings in mixed Poisson-Gaussian noise denoising.

Image	η	Method	$\sigma = 10^{-1}$		$\sigma = 10^{-2}$	
			λ_1	λ_2	λ_1	λ_2
Fluorescent Cells	1	PBCA+TV	12	0.8	12	0.7
		PBCA+Huber	17	0.7	11.9	0.7
	4	PBCA+TV	11	2.8	13	2.6
		PBCA+Huber	9.5	2.6	19.9	2
	16	PBCA+TV	12.1	11.9	31.2	6.6
		PBCA+Huber	11.2	12	26.6	6.7
Peppers	1	PBCA+TV	20	0.9	17.5	0.9
		PBCA+Huber	15	0.9	13	0.9
	4	PBCA+TV	20	2.4	29	2.4
		PBCA+Huber	10	2.8	10.2	2.7
	16	PBCA+TV	28	4.8	49	4.8
		PBCA+Huber	24.9	4.9	44	4.8
Two Code	1	PBCA+TV	3.6	1.5	3.8	1.4
		PBCA+Huber	3.5	1.4	3.6	1.4
	4	PBCA+TV	6	3.4	6.4	3.4
		PBCA+Huber	6.2	3.4	7	3.4
	16	PBCA+TV	9.2	7.6	12.8	6.6
		PBCA+Huber	10.2	7.4	14	7

Table 4.4: PSNR (dB) and SSIM values of the compared methods for denoising with mixed Poisson-Gaussian noise.

Image	η	σ	Input	PD+TV	PDHG+TV	BCA+TV	PBCA+TV	PBCA+Huber
Fluorescent Cells	1	10^{-1}	6.95	22.12	21.65	21.93	21.79	**22.24**
			0.0411	**0.4975**	0.4172	0.4423	0.4267	0.4587
		10^{-2}	7.15	22.20	21.71	22.04	21.86	**22.29**
			0.0575	**0.4992**	0.4425	0.4661	0.4670	0.4693
	4	10^{-1}	12.41	23.78	23.73	23.80	23.68	**23.91**
			0.1179	0.5687	0.5569	**0.5723**	0.5515	0.5652
		10^{-2}	13.11	24.14	24.13	24.31	24.06	**24.35**
			0.1655	0.6017	0.5959	**0.6139**	0.5918	0.6028
	16	10^{-1}	16.54	25.25	25.58	**25.73**	25.58	**25.73**
			0.2294	0.6336	0.6701	**0.6747**	0.6701	0.6677
		10^{-2}	19.18	26.50	26.62	**26.78**	26.62	**26.78**
			0.3985	0.7309	0.7346	**0.7440**	0.7347	0.7385

Table 4.4: PSNR (dB) and SSIM values of the compared methods for denoising with mixed Poisson-Gaussian noise (cont'd).

Image	η	σ	Input	PD+TV	PDHG+TV	BCA+TV	PBCA+TV	PBCA+Huber
Peppers	1	10^{-1}	3.12	19.14	19.21	19.52	19.50	**19.63**
			0.0293	0.5560	0.5130	**0.5570**	0.5379	0.5462
		10^{-2}	3.15	19.30	19.35	19.73	19.61	**19.81**
			0.0295	0.5049	0.5160	0.5537	0.5414	**0.5571**
	4	10^{-1}	8.75	21.30	21.81	**21.98**	21.95	21.90
			0.0822	0.5512	0.6106	**0.6445**	0.6152	0.6277
		10^{-2}	9.16	21.40	22.00	**22.22**	22.19	22.15
			0.0910	0.5896	0.6256	**0.6629**	0.6158	0.6482
	16	10^{-1}	13.97	24.25	24.89	24.90	25.01	**25.06**
			0.1752	0.7161	0.7127	**0.7296**	0.7189	0.7137
		10^{-2}	15.18	25.70	25.70	25.84	25.86	**25.92**
			0.2176	0.7517	0.7426	**0.7647**	0.7513	0.7479
Two Code	1	10^{-1}	2.35	16.44	15.02	16.67	**17.42**	17.25
			0.2014	0.6078	0.5551	0.5954	**0.6224**	**0.6224**
		10^{-2}	2.44	16.64	15.11	16.79	**17.61**	17.44
			0.3414	0.6375	0.5465	0.6137	0.6414	**0.6424**
	4	10^{-1}	8.15	20.59	20.10	20.46	**21.70**	21.36
			0.3439	0.7161	0.6860	0.7177	0.7326	**0.7428**
		10^{-2}	8.52	20.84	20.19	20.68	**21.97**	21.59
			0.5200	0.7457	0.6811	0.7444	0.7509	**0.7793**
	16	10^{-1}	13.43	24.33	24.71	23.95	**25.81**	25.23
			0.4541	0.8127	0.7768	0.7785	0.8167	**0.8248**
		10^{-2}	14.46	25.20	25.46	24.90	**26.68**	26.08
			0.6507	0.8312	0.7855	0.8767	0.8534	**0.8997**

4.4. Lower bound testing

In this subsection, we demonstrate that the sequence $\{w^k\}$ generated by Algorithm 3.1 has a positive and consistent lower bound. From the plot of the change in the minimum value of sequence $\{w^k\}$ shown in Fig. 4.11, it can be observed that the minimum value of sequence $\{w^k\}$ is always greater than 0.7, which indicates that Assumption 3.2 is reasonable.

5. Conclusions

Image restoration with mixed Poisson-Gaussian noise is a challenging problem in image processing. In this paper, we proposed a complete splitting algorithm to solve the TV-IC model, which is suitable for denoising and deblurring of mixed Poisson-Gaussian noise. Most importantly, the proposed approach avoids the use of the Newton iteration method to solve subproblems while solving the TV-IC model, which is a common difficulty encountered by other algorithms. Consequently, the proposed algorithm converges considerably faster than previous methods. In addition, we theoretically established the convergence of the proposed algorithm. Finally, we presented the results of numerical experiments to show that our proposed algorithm achieved better recovery performance compared to other state-of-the-art methods.

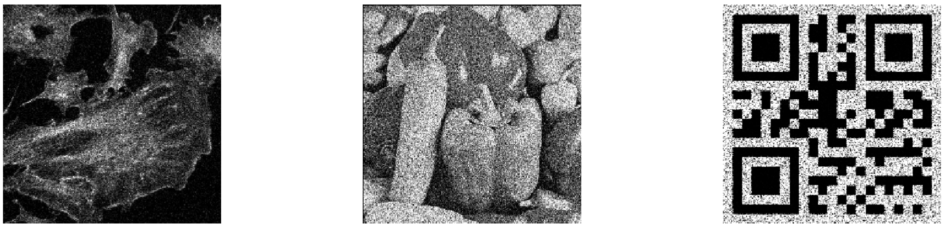

(a) Input:19.18 (b) Input:13.97 (c) Input:8.52

(d) PD+TV:26.50 (e) PD+TV:24.25 (f) PD+TV:20.84

(g) PDHG+TV:26.62 (h) PDHG+TV:24.89 (i) PDHG+TV:20.19

(j) BCA+TV:26.78 (k) BCA+TV:24.90 (l) BCA+TV:20.68

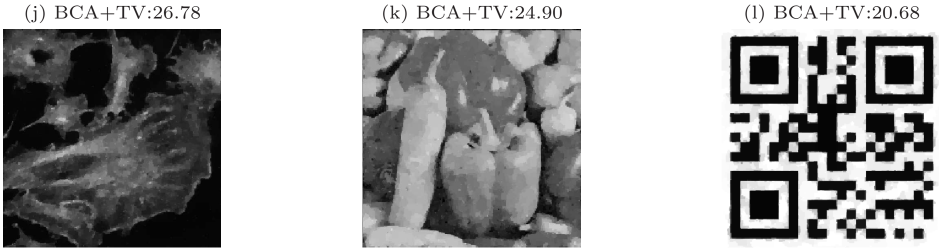

(m) PBCA+TV:26.62 (n) PBCA+TV:25.01 (o) PBCA+TV:21.97

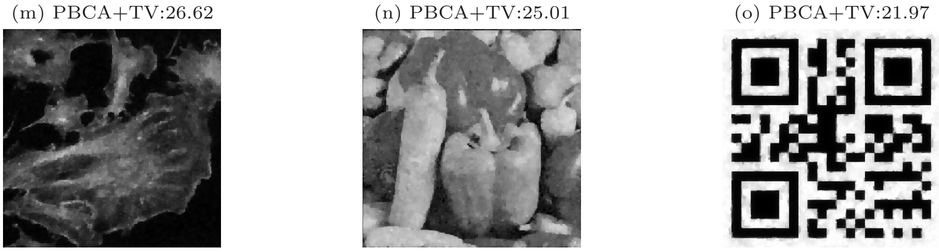

(p) PBCA+Huber:26.78 (q) PBCA+Huber:25.06 (r) PBCA+Huber:21.59

Fig. 4.10. Results of different algorithms (with PSNR(dB) below the figures) for mixed Poisson-Gaussian noise denoising. (a): "Fluorescent Cells", noise level: $\eta = 16, \sigma = 10^{-2}$; (b): "Peppers", noise level: $\eta = 16, \sigma = 10^{-1}$; (c): "Two Code", noise level: $\eta = 4, \sigma = 10^{-2}$.

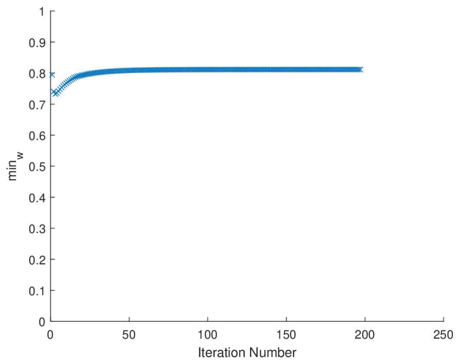

Fig. 4.11. Minimum value curves of sequence $\{w^k\}$ for the PBCA+Huber algorithm.

Acknowledgements. We would like to thank the editor and reviewers for their comments and suggestions, which helped us improve the paper. We are also thankful to Professor Huibin Chang for several helpful discussions.

This work was supported by the National Natural Science Foundations of China (Grant Nos. 12061045,12031003), by the Guangzhou Education Scientific Research Project 2024 (Grant No. 202315829), by the Guangzhou University Research Projects (Grant No. RC2023061), and by the Jiangxi Provincial Natural Science Foundation (Grant No. 20224ACB211004).

References

[1] L. Azzari and A. Foi, Variance stabilization in Poisson image deblurring, in: *2017 IEEE 14th International Symposium on Biomedical Imaging*, IEEE, (2017), 728–731.

[2] B. Begovic, V. Stankovic, and L. Stankovic, Contrast enhancement and denoising of Poisson and Gaussian mixture noise for solar image, in: *2011 18th IEEE International Conference on Image Processing*, IEEE, (2011), 185–188.

[3] M. Benning, F. Knoll, C.B. Schonllieb, and T. Valkonen, Preconditioned ADMM with nonlinear operator constraint, in: *IFIP Conference on System Modeling and Optimization*, Springer, (2015), 117–126.

[4] S. Boyd, N. Parikh, E. Chu, B. Peleato, and J. Eckstein, Distributed optimization and statistical learning via the alternating direction method of multipliers, *Found. Trends Mach. Learn.*, **3**:1 (2011), 1–122.

[5] L. Calatroni, J.C. De Los Reyes, and C.B. Schonlieb, Infimal convolution of data discrepancies for mixed noise removal, *SIAM J. Imaging Sci.*, **10**:3 (2017), 1196–1233.

[6] A. Chakrabarti and T. Zickler, Image restoration with signal-dependent camera noise, *arXiv:1204.2994*, 2012.

[7] E. Chouzenoux, A. Jezierska, J.C. Pesquet, and H. Talbot, A convex approach for image restoration with exact Poisson-Gaussian likelihood, *SIAM J. Imaging Sci.*, **8**:4 (2015), 2662–2682.

[8] M.R. Chowdhury, J. Qin, and Y. Lou, Non-blind and blind deconvolution under Poisson noise using fractional-order total variation, *J. Math. Imaging Vision*, **62**:9 (2020), 1238–1255.

[9] Q.Q. Ding, Y. Long, X.Q. Zhang, and J.A. Fessler, Modeling mixed Poisson-Gaussian noise in statistical image reconstruction for X-Ray CT, in: *in Proceedings of the 4th International Conference on Image Formation in X-Ray Computed Tomography*, (2016), 399–402.

[10] Q. Ding, Y. Long, X. Zhang, and J.A. Fessler, Statistical image reconstruction using mixed Poisson-Gaussian noise model for X-ray CT, *arXiv:1801.09533*, 2018.

[11] J. Eckstein and D.P. Bertsekas, On the Douglas-Rachford splitting method and the proximal point algorithm for maximal monotone operators, *Math. Program.*, **55**:1 (1992), 293–318.

[12] A. Foi, M. Trimeche, V. Katkovnik, and K. Egiazarian, Practical Poissonian-Gaussian noise modeling and fitting for single-image raw-data, *IEEE Trans. Image Process.*, **17**:10 (2008), 1737–1754.

[13] D. Gabay and B. Mercier, A dual algorithm for the solution of nonlinear variational problems via finite element approximation, *Comput. Math. Appl.*, **2**:1 (1976), 17–40.

[14] E. Gil-Rodrigo, J. Portilla, D. Miraut, and R. Suarez-Mesa, Efficient joint poisson-gauss restoration using multi-frame L2-relaxed-L0 analysis-based sparsity, in: *2011 18th IEEE International Conference on Image Processing*, (2011), 1385–1388.

[15] R. Glowinski and A. Marroco, Sur l'approximation, par éléments finis d'ordre un, et la résolution, par pénalisation-dualité d'une classe de problémes de Dirichlet non linéaires, *R.A.I.R.O. Analyse Numérique*, **9**:R2 (1975), 41–76.

[16] J.K. Kruschke, Bayesian data analysis, *Wiley Interdiscip. Rev. Cognit. Sci.*, **1**:5 (2010), 658–676.

[17] A. Lanza, S. Morigi, F. Sgallari, and Y.W. Wen, Image restoration with Poisson-Gaussian mixed noise, *Comput. Methods Biomech. Biomed. Eng. Imaging Vis.*, **2**:1 (2014), 12–24.

[18] M. Makitalo and A. Foi, Poisson-Gaussian denoising using the exact unbiased inverse of the generalized Anscombe transformation, in: *2012 IEEE International Conference on Acoustics, Speech and Signal Processing (ICASSP)*, IEEE, (2012), 1081–1084.

[19] M. Makitalo and A. Foi, Optimal inversion of the generalized Anscombe transformation for Poisson-Gaussian noise, *IEEE Trans. Image Process.*, **22**:1 (2012), 91–103.

[20] V. Mannam, Y.D. Zhang, Y.H. Zhu, E. Nichols, Q.F. Wang, V. Sundaresan, S.Y. Zhang, C. Smith, P.W. Bohn, and S.S. Howard, Real-time image denoising of mixed Poisson-Gaussian noise in fluorescence microscopy images using ImageJ, *Optica*, **9**:4 (2022), 335–345.

[21] Y. Marnissi, Y.L. Zheng, E. Chouzenoux, and J.C. Pesquet, A variational Bayesian approach for image restoration – application to image deblurring with Poisson-Gaussian noise, *IEEE Trans. Comput. Imaging*, **3**:4 (2017), 722–737.

[22] Y. Marnissi, Y. Zheng, and J.C. Pesquei, Fast variational Bayesian signal recovery in the presence of Poisson-Gaussian noise, in: *2016 IEEE International Conference on Acoustics, Speech and Signal Processing*, (2016), 3964–3968.

[23] J. Mei, Y. Dong, T. Huang, and W. Yin, Cauchy noise removal by nonconvex ADMM with convergence guarantees, *J. Sci. Comput.*, **74**:2 (2018), 743–766.

[24] C.A. Micchelli, L. Shen, and Y. Xu, Proximity algorithms for image models: Denoising, *Inverse Problems*, **27** (2011), 045009.

[25] F. Murtagh, J.L. Starck, and A. Bijaoui, Image restoration with noise suppression using a multiresolution support, *Astron. Astrophys. Suppl. Ser.*, **112** (1995), 179–189.

[26] G. Nemes, New asymptotic expansion for the Gamma function, *Arch. Math.*, **95** (2010), 161–169.

[27] G. Nemes, On the coefficients of the asymptotic expansion of n!, *arXiv:1003.2907*, 2010.

[28] T. Remez, O. Litany, R. Giryes, and A.M. Bronstei, Class-aware fully convolutional Gaussian and Poisson denoising, *IEEE Trans. Image Process.*, **27**:11 (2018), 5707–5722.

[29] A. Repetti, E. Chouzenoux, and J. Pesquet, A penalized weighted least squares approach for restoring data corrupted with signal-dependent noise, in: *2012 Proceedings of the 20th European Signal Processing Conference*, (2012), 1553–1557.

[30] D.D. Serafino, G. Landi, and M. Viola, ACQUIRE: An inexact iteratively reweighted norm approach for TV-based Poisson image restoration, *Appl. Math. Comput.*, **364** (2020), 124678.

[31] J.L. Starck, F.D. Murtagh, and A. Bijaoui, *Image Processing and Data Analysis: The Multiscale Approach*, Cambridge University Press, 1998.

[32] A.M. Stuart, Inverse problems: A Bayesian perspective, *Acta Numer.*, **19** (2010), 451–559.

[33] H. Sun, X.C. Tai, and J. Yuan, Efficient and convergent preconditioned ADMM for the Potts models, *SIAM J. Sci. Comput.*, **43**:2 (2021), B455–B478.

[34] Y.C. Tang, C.X. Zhu, M. Wen, and J.G. Peng, A splitting primal-dual proximity algorithm for

solving composite optimization problems, *Acta. Math. Sin. Engl. Ser.*, **33**:6 (2017), 868–886.

[35] B. Toader, J. Boulanger, Y. Korolev, M.O. Lenz, J. Manton, C.B. Schonlied, and L. Muresan, Image reconstruction in light-sheet microscopy: Spatially varying deconvolution and mixed noise, *arXiv:2108.03642*, 2021.

[36] Y. Wang, W. Yin, and J. Zeng, Global convergence of ADMM in nonconvex nonsmooth optimization, *J. Sci. Comput.*, **78**:1 (2019), 29–63.

[37] Z. Wang, A.C. Bovik, H.R. Sheikh, and E.P. Simoncelli, Image quality assessment: From error visibility to structural similarity, *IEEE Trans. Image Process.*, **13**:4 (2004), 600–612.

[38] C. Wu, J. Zhang, and X. Tai, Augmented Lagrangian method for total variation restoration with non-quadratic fidelity, *Inverse Probl. Imaging*, **5**:1 (2011), 237–261.

[39] M.C. Ye and Y.T. Qian, Mixed Poisson-Gaussian noise model based sparse denoising for hyperspectral imagery, in: *2012 4th Workshop on Hyperspectral Image and Signal Processing: Evolution in Remote Sensing*, (2012), 1–4.

[40] J. Zhang, Y.P. Duan, Y. Lu, M.K. Ng, and H.B. Chang, Bilinear constraint based ADMM for mixed Poisson-Gaussian noise removal, *Inverse Probl. Imaging*, **15**:2 (2021), 339–366.